



Efficient extraction of textile dyes using reusable acrylic-based smart polymers

Marta Guembe-García^a, Gianluca Utzeri^b, Artur J.M. Valente^b, Saturnino Ibeas^a,
Miriam Trigo-López^a, Jose Miguel García^a, Saul Vallejos^{a,*}

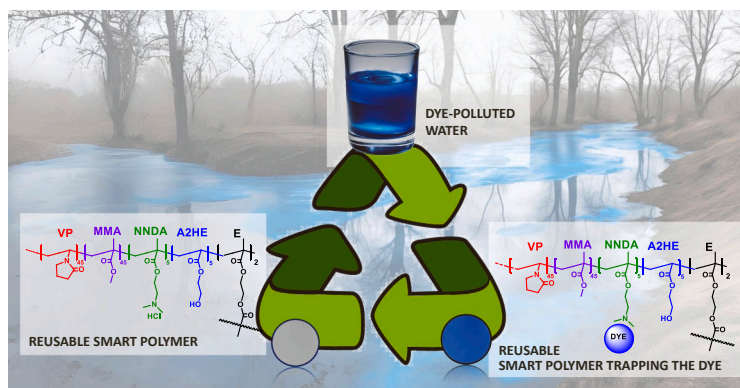
^a Departamento de Química, Facultad de Ciencias, Universidad de Burgos, Plaza Misael Bañuelos s/n, 09001 Burgos, Spain

^b CQC-IMS, Department of Chemistry, University of Coimbra, 3004-535 Coimbra, Portugal

HIGHLIGHTS

- Acrylic film with ion exchange behaviour for removing textile industry pollutants.
- Removal percentages above 90 % for anionic dyes from different families.
- Reusable, resistant and safer polymer that can be used at least 5 times.
- Suitable for both industrial and domestic washing conditions.
- POC: study of indigo carmine removal efficiency under domestic washing conditions.

GRAPHICAL ABSTRACT



ARTICLE INFO

Keywords:
Textile dyes
Smart polymer
Hydrogel
Acrylic polymers

ABSTRACT

Water pollution from industrial or household waste, containing dyes from the textile industry, poses a significant environmental challenge requiring immediate attention. In this study, we have developed a crosslinked-smart-polymer film based on 2-(dimethylamino)ethyl methacrylate copolymerized with other hydrophilic and hydrophobic commercial monomers, and its efficacy in removing 21 different textile dyes was assessed. The smart polymer effectively interacts with and adsorbs dyes, inducing a noticeable colour change. UV-Vis spectroscopy analysis confirmed a removal efficiency exceeding 90 % for anionic dyes, with external diffusion identified as the primary influencing factor on process kinetics, consistent with both pseudo-first-order kinetics and the Crank-Dual model. Isothermal studies revealed distinct adsorption behaviors, with indigo carmine adhering to a Freundlich isotherm while others conformed to the Langmuir model. Permeation and fluorescence analyses corroborated isotherm observations, verifying surface adsorption. Significantly, our proof-of-concept demonstrated the resilience of the smart-film to common fabric softeners and detergents without compromising adsorption capacity. Additionally, the material exhibited reusability (for at least 5 cycles), durability, and good thermal and mechanical properties, with T_5 and T_{10} values of 265 °C and 342 °C, respectively, a T_g of 168 °C, and a water swelling percentage of 54.3 %, thus confirming its stability and suitability for industrial application.

* Corresponding author.

E-mail address: svallejos@ubu.es (S. Vallejos).

<https://doi.org/10.1016/j.jhazmat.2024.135006>

Received 22 February 2024; Received in revised form 20 June 2024; Accepted 21 June 2024

Available online 24 June 2024

0304-3894/© 2024 The Author(s). Published by Elsevier B.V. This is an open access article under the CC BY license (<http://creativecommons.org/licenses/by/4.0/>).

Environmental implication: Dyes released during laundry processes should be classified as "hazardous materials" owing to their significant toxicity towards aquatic organisms, with the potential to disrupt ecosystems and harm aquatic biodiversity. This paper discusses the development of a novel acrylic material in film form, engineered to extract toxic anionic dyes. This study directly contributes to mitigating the environmental impact associated with the fashion industry and the domestic use of textiles. It can be implemented on both an industrial and personal scale, thereby encouraging more sustainable practices and promoting collaborative citizen science efforts towards

1. Introduction

Currently, water pollution stemming from industrial waste represents a crucial environmental challenge [1]. A primary concern is represented by the 7×10^7 tons of synthetic dyes produced worldwide with over 10,000 tons employed only in textile industry and 10 % of these dyes end up in wastewater as waste.[2] However, their presence in aquatic environments can be also related to daily domestic activities. These dyes are notorious for their high toxicity levels, which pose severe risks to human health and the integrity of aquatic ecosystems [3,4]. Their presence in water poses a risk to the environment and organisms. The colour of the dyes impedes or hinders light penetration,[5] reducing photosynthesis rates (damaging flora)[6] and consequently decreasing dissolved oxygen levels (harming fauna).[5] Additionally, many dyes are carcinogenic and/or mutagenic. They are persistent environmental pollutants, spreading through the food chain (biomagnification), meaning that the higher the trophic level, the greater the accumulated contamination in organisms.[7].

In agriculture, dyes, especially azo dyes (with 15–50 % ending up in wastewater), negatively affect soil microbiota, germination, and plant growth. This poses a significant problem for emerging agricultural sectors, such as in India, where the textile industry is prevalent (resulting in large amounts of waste) and agriculture is developing[7,8].

Regarding human health risks, these dyes cause acute toxicity through ingestion or inhalation,[9] and prolonged exposure can lead to short-term issues: skin and eye irritation;[10] medium-term: dermatitis, allergic conjunctivitis, rhinitis, occupational asthma, and various allergies;[11] and long-term: genotoxicity. Moreover, many dyes are carcinogenic, cytotoxic, mutagenic, and/or enzyme activity initiators. [7].

Given the magnitude of the problem, driven by an ever-expanding industry, it is necessary to develop new materials or techniques for the removal of these contaminants from the natural environment. The best strategy for their removal from aqueous environments is adsorption rather than degradation, as degradation products of these compounds are often more harmful than the original substances. Over the past decades, various techniques and materials have been proposed to address this issue, involving different techniques, such as: ultrafiltration [12–18], coagulation/electrocoagulation [19,20], photocatalytic degradation [21], adsorption [22–24], phytoremediation [2] and extraction using hydrogels [25,26] and aerogels [27]. The latter has been one of the mostly reported in the literature, due to its ease of preparation and application, and promising results documented for the detection and extraction of different pollutants [28]. Ibrahim et al. reported 85–90 % extraction efficiencies for various dyes using polymers based on poly(2-acrylamido-2-methylpropane) sulphonic acid, sodium polyacrylate, and chitosan [25]. In a similar vein, Alsulami et al. published analogous results using polyurethane-based foams [29].

The extraction of ionic dyes with polymeric hydrogels is predicated on the electrostatic interactions between the material and the target (dye) [30–32]. Indeed, polymeric hydrogels with positively charged structure exhibit a high affinity and removal efficiency for anionic dyes. Analogous results have been obtained in the opposite conditions [33–35].

Nevertheless, the most significant disadvantage of hydrogels is their mechanical properties, notably their often-suboptimal manageability. These drawbacks may limit their practical deployment in everyday users. Furthermore, the vast majority of the literature reviewed describes materials intended for single use, or for which reuse has not been evaluated [15]. In such scenario, possessing robust mechanical properties is imperative.

In response to this pressing issue, the present study embarks on the development and meticulous characterization of a smart polymer based on 2-(dimethylamino)ethyl methacrylate, exhibiting behaviour akin to a hydrogel membrane (with superior handling and mechanical properties). The enhancement in the mechanical properties and workability of the polymer, compared to existing alternatives, is attributed to its composition, which results in a dense material. This material format has previously yielded highly favourable outcomes in various applications [36–39] This material is specifically engineered to capture textile dyes with a remarkably high efficiency, achieving a capture rate exceeding 90 %. Herein, we can categorize the material reported in this work as a smart material based on the definition reported by García et al. [40], that is, a material capable of interacting with a target (dye) through a specific mechanism (ion exchange, electrostatic interaction) and generating a precise response (extraction of the dye and consequent coloration of the material). This 'material's pivotal and innovative characteristic is its potential for reuse and sustained durability (Fig. 1) since its adsorption properties are not affected by load-wash cycles. These features are crucial for two reasons. Firstly, it aims to minimize the generation of additional waste in the process of dye pollution remediation. Secondly, with robust mechanical properties, the material can be feasibly used by non-specialists, including everyday consumers, allowing for potential application at a household level. Consequently, this approach addresses the pollution issue comprehensively and fosters sustainability in pollution management practices.

While preceding research was predominantly concentrated on the utilization of hydrogel-type materials for the extraction of both cationic and anionic dyes from aqueous solutions [25], our research does not confine itself to the investigation of a singular dye family. Rather, it extends its exploration to evaluate the efficacy of the novel polymeric material across a diverse spectrum of dye families. This includes, but is not limited to, families such as azo dyes, organometallic dyes, triarylmethane-derivatives, xantene-derivatives, anthraquinone structures, benzothiazolium salts, biindolinylidene-derivatives, quinone-imine structures and carbocyanine based dyes.

The 21 dyes selected for this study, listed below, include both cationic and anionic types and are predominantly used in the textile industry (Table 1): Mordant Blue 29, Mordant Blue 3, Rhodamine-B, Alizarin Red S, Rose Bengal, Congo Red, Basic Yellow, Brilliant Green, Prussian Red, Indigo Carmine, Acid Yellow 36, Methylene Blue, Pina-cyanol Chloride, Xylenol Orange, Crystal Violet, Direct Black 38, Orange GR, Black 5, Sunset Yellow, Navy Blue Erionyl R, and Reactive Orange 7. This flexible and inclusive approach not only highlights the 'material's adaptability but also enhances its potential for widespread use in different industrial and household settings.

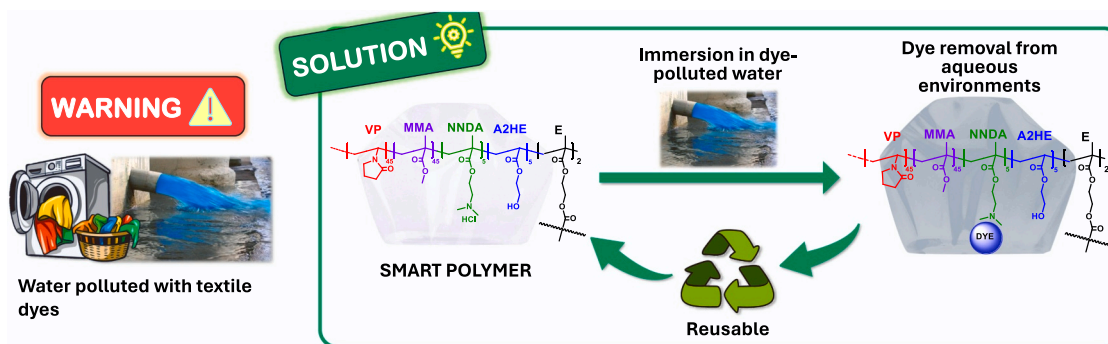


Fig. 1. Table of contents.

2. Experimental

2.1. Materials

All materials and solvents were commercially available and used as received unless otherwise indicated. The following materials and solvents were used: methylmethacrylate (MMA) (Merck, 99 %), 1-vinyl-2-pyrrolidone (VP) (Acros Organic, 99 %), *N,N*-dimethylaminoethyl methacrylate (NNDA) (Aldrich, 98 %), 2-hydroxyethyl acrylate (2HEA), (Aldrich, 96 %), ethylene glycol dimethacrylate (E) (Aldrich, 98 %), azo-bis-isobutyronitrile (AIBN, Aldrich, 98 %) was recrystallized twice from methanol, hydrochloric acid (VWR, 37 %), Mordant Blue 29 (MP, 100 %), Mordant Blue 3 (Acros Organic, 100 %), Thymol blue (Alfa Aesar, 100 %) Rhodamine-B (Alfa Aesar, 100 %), Alizarin red S (Alfa Aesar, 100 %), Rose Bengal (Thermo scientific, 100 %), Congo Red (Thermo scientific, 100 %), Basic yellow (Alfa Aesar, 75 %), Brilliant green (Thermo scientific, 100 %), Prussian red (Thermo scientific, 100 %), Indigo carmine (TCI, >95 %), Acid Yellow 36 (TCI, 100 %), Methylene Blue (TCI, >70), Pinacyanol chloride (TCI, >90 %), Xylenol orange (TCI, 100 %), Crystal violet (TCI, 100 %), Direct Black 38 (TCI, 100 %), Orange GR (TCI, >97 %), Black 5 (Sigma Aldrich, ≥50 %), Sunset yellow (Cayman Chemical Company, 100 %), Navy blue Erionyl R (Aldrich, 50 %), Reactive Orange 7 (Sigma Aldrich, ≥70 %), Eosin Y (Sigma Aldrich, ≈99 %), Fluorescein (Fluka, 100 %), Indigo (TCI, >97 %).

For the proof of concept, commonly used laundry products such as detergent and fabric softener were employed. Photographs of both products and their respective ingredient lists can be found in the Electronic Supplementary Information (ESI-Section S1, Figure S1a and S1b).

2.2. Instrumentation and general methods

Thermal properties of the material were evaluated employing different analytical methodologies. Thermogravimetric analysis (TGA) was conducted on 10 – 15 mg samples under synthetic air and a nitrogen atmosphere, utilizing a *TA Instruments Q50 TGA* analyser with a heating rate of 10 °C min⁻¹. Differential scanning calorimetry (DSC) involved 10 – 15 mg samples under a nitrogen atmosphere, analysed using a *TA Instruments Q200 DSC* analyser with a heating rate of 20 °C min⁻¹.

The water-swelling percentage (WSP), at 20 °C, was calculated using the formula: $WSP = 100 \times [(w_s - w_d) / w_d]$, where w_d represents the weight of a dry sample film, and w_s denotes its weight post-swelling.

UV/Vis spectra were acquired employing a *Hitachi U-3900 UV/Vis* spectrophotometer. The synthesized 'materials' infrared spectra (FT-IR) were obtained using a *JASCO FT-IR 4200* spectrometer in the 4000–400 cm⁻¹ range.

Inductively coupled plasma mass spectrometry (ICP-MS) measurements were recorded on a 7500 ICP-MS spectrometer (Agilent, Santa Clara, CA, USA).

Field Emission Scanning electron microscopy (FESEM) was carried out using a model GeminiSEM560, ZEISS. Parallely, Energy Dispersive X-ray Spectrometry (EDXS) analysis was conducted using UltimMax Extreme (Oxford). In both case, films were dried, freeze fractured, and gold coated in vacuum to ensure the electrical conductivity.

RAMAN spectra were recorded with a confocal AFM-RAMAN model Alpha300R – Alpha300A AFM from WITec, using a laser radiation of 532 nm, at magnifications of 100 ×. All spectra were taken at room temperature.

The powder X-ray diffraction (PXRD) patterns were obtained using a diffractometer (D8 Discover Davinci design, Bruker Corporation, Billerica, Massachusetts, USA) operating at 40 kV, using Cu(K α) as the radiation source (1.54 Å), a scan step size of 0.05°, and a scan step time of 2 s

Tensile properties analysis was conducted using samples measuring 5 × 9.44 × 0.122 mm, employing a Shimadzu EZ Test Compact Table-Top Universal Tester at a speed of 1 mm/min⁻¹ (EZ Test EZ-LX, Shimadzu, Kyoto, Japan).

Samples for PXRD and ICP-MS tests were prepared by milling the polymeric materials using a ball mill machine (MM400, Retsch, Haan, Germany). The equipment was operated at a frequency of 25 Hz for 5 min, and the capsules were pre-immersed in liquid nitrogen for 20 min.

Total nitrogen (TN) was measured on an autoanalyzer TOC-V CSN (Shimadzu Corp., Kyoto, Japan).

For the calculation of the size of the dye molecules, the Avogadro software (Version 1.2.0) was utilized.

2.3. Specific methods

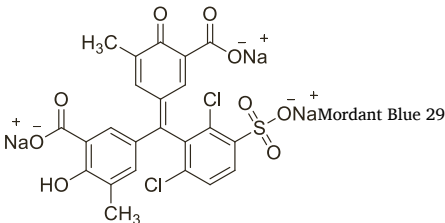
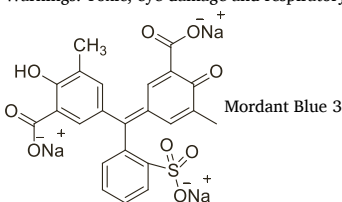
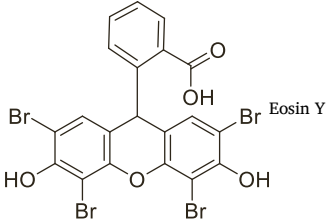
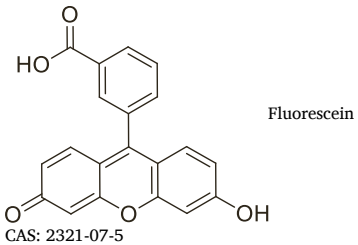
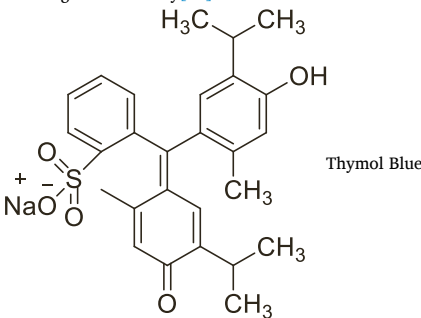
2.3.1. Preparation of the polymeric material

The procedure followed was that described by Vallejos et al., with modifications.[41] The main material was synthesized through radical polymerization using four commercial copolymers: two hydrophilic ones (vinylpyrrolidone, VP, and 2-hydroxyethyl acrylate, 2HEA), one hydrophobic (methyl methacrylate, MMA), and a fourth one containing a tertiary amine capable of protonation (*N,N*-dimethylaminoethyl methacrylate, NNDA), in molar proportions of 45/45/5/5 (VP/MMA/NNDA/2HEA). Additionally, 1 % (w/w) of AIBN as a radical thermal initiator, and 2 mol% of ethylene glycol dimethacrylate (E) as the cross-linking agent were added to the mixture. Bulk radical polymerization was conducted within a silanized glass mold of 100 μm thickness, under an oxygen-depleted atmosphere at a temperature of 60 °C overnight. This procedure yielded the membrane denoted as F1, which subsequently underwent a triple cleaning process with water, acetone, and water again.

Following this, the tertiary amine group within NNDA was protonated through the immersion of F1 in a 3.7 % aqueous HCl solution for 1 h, resulting in the formation of membrane F2. The residual HCl was removed by immersing membrane F2 three times in distilled water, with

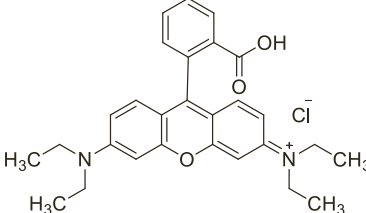
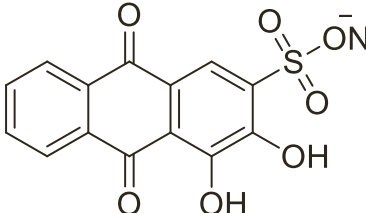
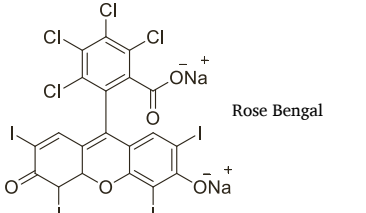
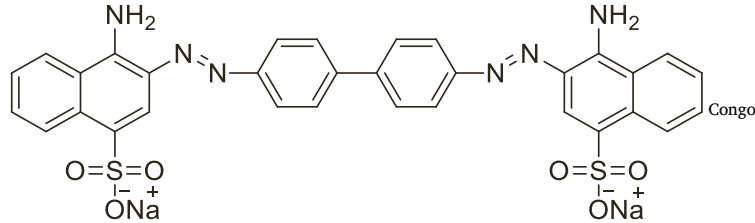
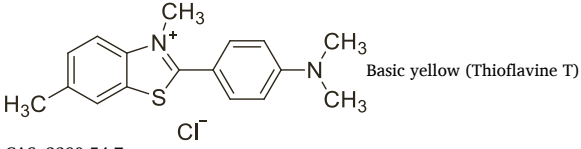
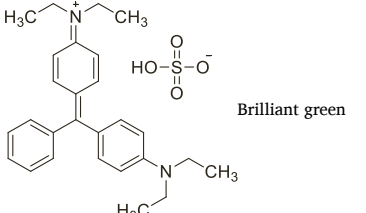
Table 1

List of dyes used in the preliminary study, indicating CAS number, common name, chemical formula, dye family to which they belong, obtained q_e , and removal percentage.

Dye N°	Dye	Family	pKa	q_e , mg/g	Dye removal %
1	 <p>Mordant Blue 29</p> <p>CAS: 1667-99-8 Warnings: Toxic, eye damage and respiratory irritation[56]</p>	Triarylmethane	-2.2, -1.2, 2.25, 4.88, 11.75[57]	27.65	98.20
2	 <p>Mordant Blue 3</p> <p>CAS: 3564-18-9 Warnings: Toxic limit 2000 mg/Kg ([58])</p>	Triarylmethane	0, 1.83, 5.74, 11.83[59]	28.29	99.53
3	 <p>Eosin Y</p> <p>CAS: 15086-94-9 Warnings: Toxic and mutagenic[60]</p>	Xhantene	2.9, 4.5[61]	*	*
4	 <p>Fluorescein</p> <p>CAS: 2321-07-5 Warnings: Low toxicity[62]</p>	Xhantene	2.2, 4.4, 6.7 [61]	*	*
5	 <p>Thymol Blue</p> <p>CAS: 76-61-9 Warnings: Damage to the digestive tract, respiratory tract and skin[63]</p>	Triarylmethane	1.76, 9.05[64]	*	*

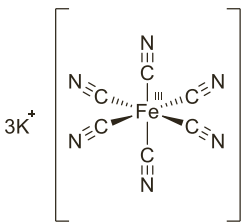
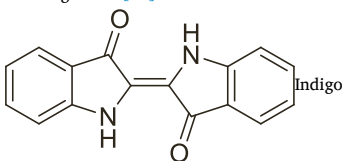
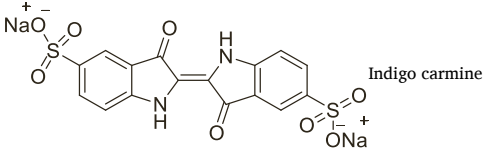
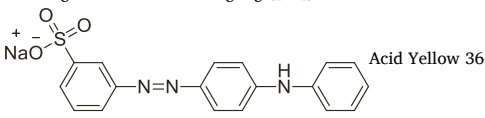
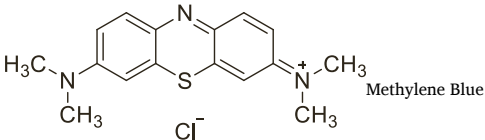
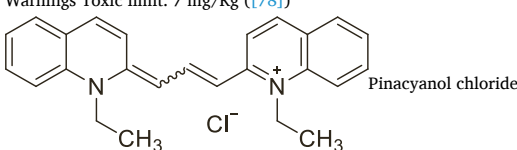
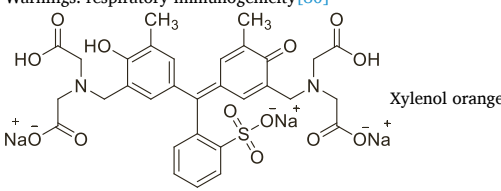
(continued on next page)

Table 1 (continued)

Dye N°	Dye	Family	pKa	q _e , mg/g	Dye removal %
6	 <p>Rhodamine-B</p> <p>CAS: 81-88-9 Warnings: Toxic limit: 14 a 24 mg/L ([65])</p>	Xhantene	3.7[66]	6.25	22.00
7	 <p>Alizarin red S</p> <p>CAS: 130-22-3 Warnings: Toxic limit: 70 mg/Kg ([67])</p>	Anthroquinone	4.5, 11[61]	27.87	98.63
8	 <p>Rose Bengal</p> <p>CAS: 632-69-9 Warnings: Eye damage and skin irritation[63]</p>	Xhantene	3.9, 4.7[68]	27.02	96.10
9	 <p>Congo</p> <p>Red</p> <p>CAS: 573-58-0 Warnings: Toxic limit: 3.11 mg/L ([69])</p>	AZO	4.1[61]	17.43	61.33
10	 <p>Basic yellow (Thioflavine T)</p> <p>CAS: 2390-54-7 Warnings: Acute oral toxicity, eye damage and skin irritation.[70]</p>	Benzothiazolium salts	1.8, 4.9[71]* *	1.83	6.44
11	 <p>Brilliant green</p> <p>CAS: 633-03-4 Warnings: Toxic limit: 50 mg/L ([72])</p>	Triarylmethane	2.62, 4.93[73]	13.87	48.81

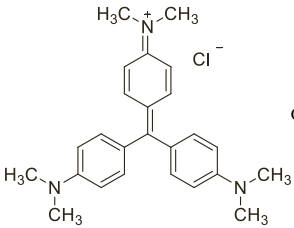
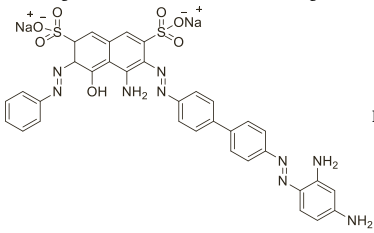
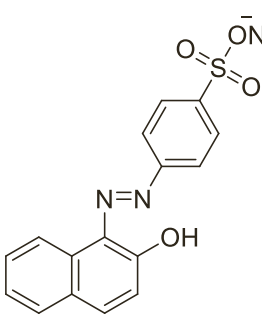
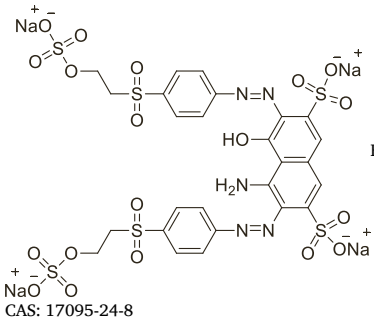
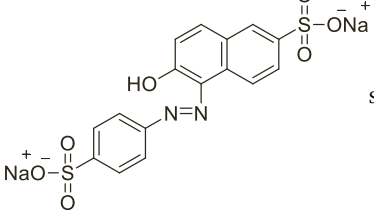
(continued on next page)

Table 1 (continued)

Dye N°	Dye	Family	pKa	q _e , mg/g	Dye removal %
12	 <p>Prussian red (Potassium hexacyanoferrate III)</p> <p>CAS: 16746-66-2 Warnings: Toxic[74]</p>	Organometallic	* **	28.49	99.61
13	 <p>Indigo</p> <p>CAS: 482-89-3 Warnings: Toxic limit: 5000 mg/Kg ([75])</p>	Biindolylidene	10.1[71] * *	*	*
14	 <p>Indigo carmine</p> <p>CAS: 860-22-0 Warnings: Toxic limit: 500 mg/Kg ([76])</p>	Biindolylidene	8.8[71] * *	29.28	98.58
15	 <p>Acid Yellow 36</p> <p>CAS: 587-98-4 Warnings: Toxic and carcinogenic[77]</p>	AZO	2.12[61]	27.39	96.36
16	 <p>Methylene Blue</p> <p>CAS: 122965-43-9 (solution 61-73-4) Warnings: Toxic limit: 7 mg/Kg ([78])</p>	Quinone-imine	3.8[79]	3.25	11.44
17	 <p>Pinacyanol chloride</p> <p>CAS: 2768-90-3 Warnings: respiratory immunogenicity[80]</p>	Carbocyanine	3.5[81]	17.76	62.47
18	 <p>Xylenol orange</p> <p>CAS: 1202864-39-8 Warnings: Toxic[82]</p>	Triarylmethane	2.6, 6.4, 6.5, 10.5, 12.3[61]	27.45	96.62

(continued on next page)

Table 1 (continued)

Dye N°	Dye	Family	pKa	q _e , mg/g	Dye removal %
19	 <p>Crystal violet</p> <p>CAS: 548-62-9 Warnings: Toxic, Genotoxic and Carcinogenic[83]</p>	Triarylmethane	9.4[61]	2.17	7.62
20	 <p>Direct Black 38</p> <p>CAS: 1937-37-7 Warnings: Toxic limit: 1500 mg/L ([84])</p>	AZO	4.2, 5.1, 5.2, 9.8, 12. 12.4 [71] * *	8.71	30.64
21	 <p>Orange GR</p> <p>CAS: 633-96-5 Warnings: Carcinogens[85]</p>	AZO	8.26, 11.4[61]	27.44	96.55
22	 <p>Black 5</p> <p>CAS: 17095-24-8 Warnings: Toxic limit: 28 mg/L ([8])</p>	AZO	3.5, 4.7, 9.4 [71] * *	27.30	96.04
23	 <p>Sunset yellow</p> <p>CAS: 2783-94-0 Warnings: Toxic limit: 2.5 mg/Kg ([86])</p>	AZO	6.1, 11.8[87]	25.63	90.16

(continued on next page)

Table 1 (continued)

Dye N°	Dye	Family	pKa	q _e , mg/g	Dye removal %
24	<p>Navy blue Erionyl R (Acid Blue 113)</p> <p>CAS: 3351-05-1 Warnings: Acute toxic[88]</p>	AZO	4.3, 11.5 [71]* *	27.47	96.63
25	<p>Reactive Orange 7</p> <p>CAS: 12225-83-1 Warnings: Toxic limit: 2.5 mg/Kg ([89])</p>	AZO	5.4, 13.2[71] * *	27.65	98.20

* The experiments were not conducted due to the low or negligible water solubility of the dye.

** Theoretically calculated pKa values.

*** Without theoretical or experimental values.

each immersion lasting for 5 min. The chemical structure and a photograph of the material are illustrated in Figs. 2a and 2b, respectively.

2.3.2. Removal and kinetic study by UV-Vis spectroscopy

A prior calibration was performed using solutions of 2.5 to 60 mg L⁻¹ for each dye.

For these studies, F2 was punched into 10 mm diameter discs and then immersed in 3.5 mL of solutions with a concentration of 50 mg L⁻¹ of each dye. The UV-Vis absorption spectrum (200–900 nm) was measured every 15 min for 24 h. To calculate the percentage of dye removal, the following formula was employed:

$$\text{Dye removal\%} = \frac{C_0 - C_F}{C_0} \times 100 \quad (1)$$

where C_0 and C_F are the initial and the final concentrations of the dye in the solution.

Consistent with previous studies about adsorption processes in acrylic polymers [42], the analysis of the obtained results assumed a pseudo-first-order kinetic:

$$q_t = q_e(1 - e^{-k_1 t}) \quad (2)$$

where, q_t (mg g⁻¹) is the milligrams of adsorbate per gram of adsorbent at a time t , q_e (mg g⁻¹) is the amount of dye adsorbed at equilibrium and k_1 is the first-order kinetic constant. For the diffusion study, the Crank-Dual model was employed:

$$\frac{q_t}{q_e} = 1 - \sum_{n=1}^{\infty} \frac{2B_n^2 \exp(-\beta_n^2 D_s t / l^2)}{\beta_n^2 (\beta_n^2 + B_i^2 + B_i)} \quad (3)$$

$$\beta_n \tan \beta_n = B_i \quad (4)$$

B_i is Biot number, i.e., ratio of external film diffusivity to intra-particle diffusivity, D_s (cm² min⁻¹) is the diffusion coefficient of sorbate within the sorbent and k_f (cm min⁻¹) are external or film mass transfer coefficient.

2.3.3. Isotherm study by UV-Vis spectroscopy

The isotherm study was conducted through two experimental procedures, A and B. In the case of procedure A, the concentration of the dye solution was kept constant at 50 mg L⁻¹, and the size of the smart polymer disc was varied (3 to 14 mm in diameter). For procedure B, the disc size was kept at 10 mm, and different concentrations of dye (2.5 to 60 mg/L) were used. In both cases, each solution was measured prior to introducing the F2 disk, and approximately 24 h elapsed after introducing the F2 disk. The obtained results were analysed using Freundlich and Langmuir isothermal models. When adsorption equilibrium is reached, the solute is distributed between the solution and the solid, where q_e can be computed by the following equation:

$$q_e = \frac{C_0 - C_e}{w} V \quad (5)$$

where V (L) is the volume of the solution used, and w is the mass in grams of the adsorbent.

Langmuir was the first proposing an adsorption theory on a flat surface from a kinetic perspective [43,44]. The model suggests adsorption in a single layer on the surface, considering a finite number of active sites at identical energy. Adsorption takes place on these centres with only one molecule per site. The following equation describes this model:

$$q_e = \frac{q_{\max} K_L C_e}{1 + K_L C_e} \quad (6)$$

where q_{\max} (mg/g) is a constant indicating the maximum adsorption capacity in the monolayer, and K_L (L/mg) defines the affinity of the adsorbate for the adsorbent. These two constants allow calculating the thermodynamic equilibrium constant, K_c , from their product:

$$K_c = K_L q_{\max} \quad (7)$$

On the other hand, Freundlich isotherm model is an empirical equation, assuming that the adsorbent surface is energetically heterogeneous, formed by different adsorption sites with characteristic energies [45]. Differently to the Langmuir model, the Freundlich isotherm considers the formation of adsorbate-adsorbate interactions with

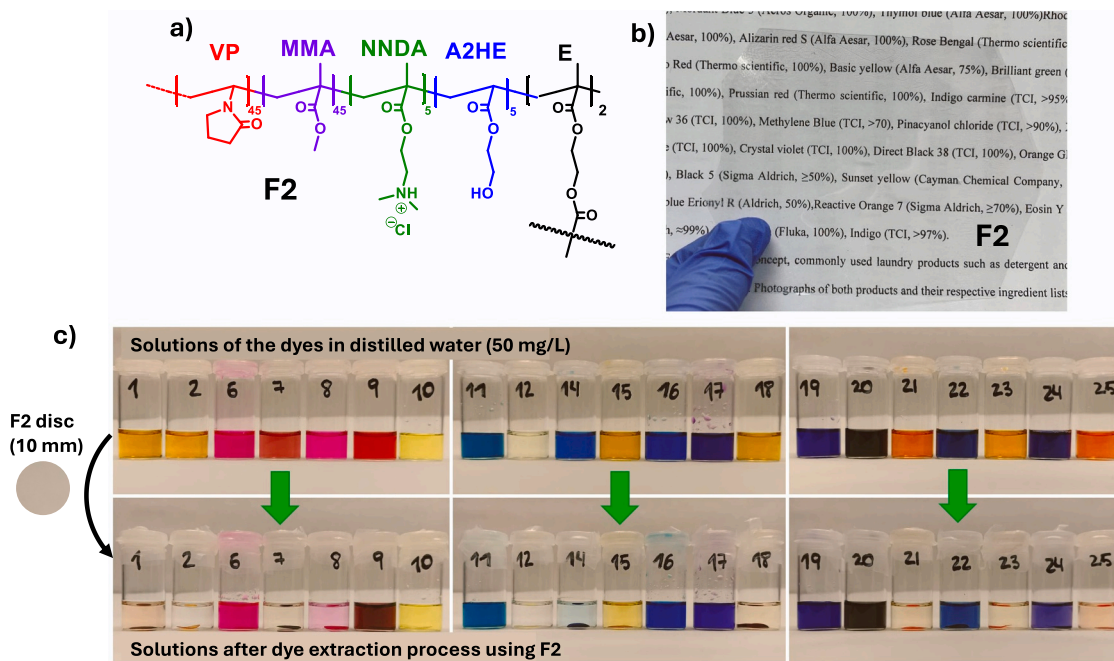


Fig. 2. a) Selected formulation for the manufacture of the smart polymer. b) Photograph of the prepared membrane. c) Solutions of 3.5 mL dyes at an initial concentration of 50 ppm (above) and once the adsorption process is completed (below).

multilayer formation:

$$q_e = K_F C_e^{1/n} \quad (8)$$

where K_F ($\text{mg/g} (\text{mgL}^{-1})^{-1/n}$) and n represents the capacity and intensity of adsorption, respectively.

2.3.4. Permeation analysis by UV-Vis spectroscopy

The permeation study was conducted by time-lag analysis using a system consisting of horizontal communicating vessels, as described in reference [46]. In this setup, the material under investigation (F2) serves as a barrier between the channel connecting the two vessels. Cutting the membrane in circular shape of a defined diameter permits obtaining a defined permeation area of 2 cm^2 . Vessel "A" contains Milli-Q ultrapure water, while vessel "B" holds an aqueous dye solution of 50 mg/L . The permeation process was monitored by measuring the absorbance at the λ_{max} of the solution in the vessel "A" over time, using a UV-visible spectrophotometer (UV-2600i, Shimadzu, Germany). Calibration curves were generated for each dye within the analytical range of $0\text{--}60 \text{ mg/L}$. The F2 membrane has a thickness ($L = 100 \mu\text{m}$) and permeation area ($A = 2 \text{ cm}^2$), the cell volume ($V = 200 \text{ mL}$), and the concentration of dye in the donor cell ($C_{\text{dye}} = 50 \text{ mg L}^{-1}$). The diffusion coefficient (D) and permeation coefficient (P) are computed using the following equations:

$$D = \frac{L^2}{\theta} \quad (9)$$

$$P = \frac{(V \times S \times L)}{A \times C_0} \quad (10)$$

where θ (s) is the time-lag, and S represents the slope of the curve obtained by plotting the permeant concentration as a function of time, observed at the steady-state condition. Consequently, we determined a coefficient of partition ($K_p = P/D$), which indicates the affinity of the permeate to the membrane.

After the permeation analysis, the membranes were dried in a desiccator and successively used for the fluorescence analysis on both sides of the membrane: side in contact with vessel "A"-pure water and vessel "B"-dye solution.

2.3.5. Fluorescence study

Besides the visible absorbance of dyes, most dye molecules also show photoluminescence. This property has been employed in several fields [47–51].

In this study, we exploit this property to obtain complementary qualitative information that allows for a better understanding of the adsorption process in terms of the adsorbent-adsorbate interaction. F2 membranes used in permeation experiments were characterized by fluorescence. Measurements were performed using *Horiba-Jobin-Ivon SPEX Fluorolog 3.22* spectrofluorometer and all fluorescence spectra were corrected for the wavelength response of the system. In general, depending on the dye analysed three different wavelength (nm) of excitation was employed (e.g. $\lambda_1 = 420 \text{ nm}$, $\lambda_2 = 520 \text{ nm}$ and $\lambda_3 = 600 \text{ nm}$).

2.3.6. Reusability study

The evaluation of material reusability was conducted using adsorption and desorption cycles, following published strategies with modifications [52]. An F2 disc of 10 mm diameter was immersed in 3.5 mL of dye 14 (10 mg/L) overnight. Subsequently, the disc was removed from the solution, and the absorbance of the solution was measured. Desorption of dye 14 was achieved by immersing the disc in 5 mL of $1 \text{ mol L}^{-1} \text{ NaOH}$. To obtain complete desorption, the disc was immersed in the basic solution overnight, preceded by a wash in 5 mL of distilled water for 5 min . Once the dye was removed, the disc was immersed in 10 mL of a $4\% \text{ HCl}$ solution for 1 h and washed three times with 5 mL of distilled water for 15 min each time. This cycle of use/washing was repeated 5 times.

2.3.7. TOC

The total nitrogen content (TN) was measured in the solution before and after treatment with F2. For this study, Dye 12 was selected due to its high nitrogen content and because it is the only organometallic dye. Additionally, Dye 14 was chosen for its relevance in the textile industry. Solutions of both dyes were prepared at a concentration of 50 ppm , and the total nitrogen content was studied. Subsequently, 3.5 mL of this solution was taken, and a 10 mm diameter F2 disc was immersed in it at 25°C for 12 h . A total of 60 tests were conducted under these conditions

to obtain a sufficient quantity for the experiment. Finally, the resulting solutions from the extraction process of each dye were collected and homogenized for total nitrogen measurement.

The remaining F2 disks were used for ICP-MS, PXRD, RAMAN, and SEM analyses.

2.3.8. Proof of concept: evaluation of the smart polymer under real-life-simulated conditions

Our material can be potentially utilized in both industrial and domestic environments. Therefore, we aimed to assess the efficiency of the smart polymer under conditions akin to those potentially encountered in a household washing machine, considering the composition of the washing solution. This assessment aligns with the material's prospective applications, such as coating for drainage pipes or purification membranes. The 10 mm diameter disc of F2 material was immersed in a solution of 3.5 mL of tap water, 10 μ L of fabric softener, and 10 μ L of laundry detergent. The UV-Vis absorption spectrum (200–900 nm) was measured every 15 min for 24 h.

3. Results and discussion

3.1. Characterization of the material

The handleability of a material is a highly significant property, mainly when its final applications are focused on domestic use. From a theoretical perspective, the handleability of a material is primarily associated with its mechanical and thermal properties. These properties must be maintained under the intended working conditions for the material. For instance, industrial textile washes are conducted at 75 °C. In this case, the TGA analysis reveals that T_5 and T_{10} (temperatures at which a weight loss of 5 % and 10 % is observed, respectively) have values of 265 °C and 342 °C, respectively.[53] These values are commonly found in similar acrylic polymers and ensure the polymer's thermal stability in industrial applications and processes using steam or even boiling water. Furthermore, characterization through DSC indicates a glass transition temperature (T_g) of 168 °C, which, combined with the TGA results, confirms the material's suitability for the proposed application.

From a mechanical perspective, the Young's modulus of F1 was analyzed immediately after demolding, yielding a value of 435 \pm 48 MPa. This result is consistent with the moduli reported in the literature for similar materials [54].

The F2 material was analyzed by FT-IR, which showed typical signals for this type of polymer, such as the carbonyl stretching signals of the ester (1719 cm^{-1}) corresponding to MMA, NNDA, and 2HEA, the amide (1663 cm^{-1}) corresponding to VP, and the broadband associated with the -OH stretching band of 2HEA (3428 cm^{-1}). IR, TGA, and DSC graphs are provided in the Electronic Supplementary Information (ESI-Section S2).

On the other hand, the material, F2 presents a water swelling percentage (WSP) of 54 \pm 3 %, derived from its modified composition, enabling interaction of the material with the adsorbate and enhancing its adsorption and retention capabilities.

It is crucial to note that 3 of the 4 monomers used in the synthesis of the material are hydrophilic, thereby producing materials that exhibit significant swelling in water. This characteristic is beneficial as it facilitates the entry of the targets (dyes) into the three-dimensional structure of the material, but only up to a certain extent. Excessive swelling of the material can severely compromise its manageability. This is why the role of the cross-linker becomes essential. In our previous studies [55], the amount of cross-linker typically used is 0.1 mol/mol%. In these studies, the amount of hydrophobic monomers was < 50 mol%, which controls water swelling. In this case, since the mol% of hydrophilic monomers exceeds 50 mol%, an increase of ethylene glycol dimethacrylate (E) cross-linking agent to 2 mol%, to achieve balanced water swelling and maintain the material's handleability, has been made.

From the perspective of polymer material design, the inclusion of groups susceptible to protonation is crucial for dye removal. These groups can harbor positive charges, allowing for the exchange of anions—specifically, exchanging chlorides for anionic dyes. Additionally, the presence of other monomers is essential for ensuring the material possesses suitable properties, such as manageability. Put differently, if the material were composed entirely of NNDA, its dye absorption capacity would be much greater. However, this would likely come at the expense of mechanical properties due to the material's significantly increased hydrophilicity. Thus, striking a balance is essential. Furthermore, the dense nature of the material is highly relevant, enabling its reuse without sacrificing mechanical properties or dye extraction capability.

3.2. Preliminary results. Removal % and q_e

Preliminary tests were conducted with 25 different dyes. However, dyes 3, 4, 5, and 13 were excluded from the study due to their lack of solubility in water. Table 1 shows each dye's chemical structures, common names, CAS numbers, pKa, q_e , and removal %.

In Fig. 2c, the solutions of the 21 dyes can be observed both before introducing the material and after the adsorption process. Consistent with the data presented in Table 1, it becomes evident that the highest adsorption efficiencies (dye removal % > 90) are associated with dyes 1, 2, 7, 8, 12, 14, 18, 21, 23, 24, and 25. Conversely, lower adsorption percentages (7 < dye removal % < 63) are observed for dyes 6, 9, 10, 11, 16, 17, 19, and 20.

As the literature describes, materials with a positive charge, such as F2, exhibit two potential interaction mechanisms: ion exchange [90] and/or electrostatic interaction [13,16,18,22]. In the first scenario, an exchange occurs between the H⁺ ions of the membrane and the dye components. In the second scenario, the positively charged matrix attracts the dyes in their anionic (deprotonated) state. In both cases, the pH solution plays an important role. Previous studies have shown that, in the case of electrostatic interactions, neutral pH values (7–8) yield the most effective adsorption results [22]. In this instance, we are dealing with electrostatic interaction behaviour, where the positively charged membrane can adsorb dyes in their deprotonated (anionic) form at the working pH. However, the membrane would not work for dye extraction at pH levels where the NNDA monomer is deprotonated, specifically at pH levels above 8. In this situation, the NNDA monomer would deprotonate and release the dye back into the medium. This phenomenon has been leveraged as a strategy to design the material's reuse cycles: in its protonated form, the membrane extracts dyes, and in its deprotonated form, it releases them.

3.3. Kinetic study

After the preliminary study of dye removal percentages, we proceeded with an in-depth investigation, selecting one representative from each dye family, except for the triarylmethane family, for which two were chosen. Specifically, the dyes with the highest dye removal percentages were chosen, namely dyes 1 and 18 (triarylmethane family), dye 7 (anthraquinone family), dye 8 (Xanthene family), dye 12 (organometallic family), dye 14 (biindolinylidene family), and dye 21 (azo family).

The adsorption processes in solution can be divided into four stages. The comprehension of this phenomenon requires distinguishing between two external regions (outside the membrane): the area that encircles the material and the remainder of the solution. The initial stage is rapid, and involves the migration of the solute from distant zones towards the vicinity of F2, while the second stage concerns the migration from the vicinity of F2 to its surface. The intraparticle diffusion represents the third stage, and the final one involves the solute's adsorption onto the adsorbent's active sites. Various mathematical models exist for interpreting the results of adsorption monitored through UV-Vis

Table 2

Kinetic parameters obtained through nonlinear least squares fitting to Eq. 2, $[Dye]_0 = 50 \text{ mg/L}$, and parameters obtained through nonlinear least squares fitting of the Crank-Dual model reported in Eq. 3.

Nonlinear Least Squares Fitting					
Dye N°	$k_1 \cdot 10^5, \text{s}^{-1}$		$q_e, \text{mg}_{\text{dye}}/\text{g}_{\text{F2}}$		R^2
18	4.45	± 0.03	26.05 ± 0.05		0.999
14	5.47	± 0.05	29.75 ± 0.09		0.998
7	5.92	± 0.02	27.99 ± 0.03		0.999
21	6.48	± 0.03	28.74 ± 0.03		0.999
1	7.18	± 0.04	27.48 ± 0.05		0.999
8	8.70	± 0.20	26.00 ± 0.10		0.984
12	9.42	± 0.04	28.63 ± 0.02		0.999
Crank-Dual model					
Dye	$D_s \cdot 10^{12}, \text{m}^2/\text{s}$	$k_f \cdot 10^9, \text{m}/\text{s}$	$q_e, \text{mg}/\text{g}$	B_i	R^2
18	0.87 ± 0.07	2.49 ± 0.02	25.87 ± 0.03	0.143 ± 0.002	0.9996
14	1.04 ± 0.02	3.11 ± 0.03	29.49 ± 0.06	0.149 ± 0.004	0.9993
7	1.19 ± 0.08	3.21 ± 0.02	27.92 ± 0.02	0.134 ± 0.002	0.9998
21	1.29 ± 0.01	3.53 ± 0.02	28.67 ± 0.03	0.137 ± 0.002	0.9996
1	1.54 ± 0.01	3.67 ± 0.04	27.51 ± 0.05	0.119 ± 0.003	0.9990
8	1.00 ± 8.00	5.00 ± 3.00	25.86 ± 0.08	0.200 ± 0.900	0.9900
12	1.94 ± 0.02	4.99 ± 0.04	28.62 ± 0.02	0.128 ± 0.002	0.9993

spectroscopy, such as the pseudo-first-order kinetic and the Crank-Dual models. The former assumes that the fourth stage is the rate-determining step, while the latter suggests that the most crucial stages are the second and the third, related to diffusion. The first model enables us to determine the percentage of adsorption at any given time, whereas the Crank-Dual model allows us to elucidate the kinetic mechanism of adsorption.

Table 2 displays the results of the kinetic parameters calculated using each model, i.e., the pseudo-first-order kinetic model and the Crank-Dual model, respectively (the corresponding graphs can be found in the ESI-Section S3 Figures S7c-S12c, and S7d-S12d).

The values of $B_i < 1$ indicates that external diffusion is the dominant factor influencing the overall process rate [91–93]. This finding aligns with previous studies on similar materials [42].

Considering that the geometrical dimensions of the membrane are strictly controlled, we can observe that k_1 and k_f follow the same trend, confirming that the external diffusion is the dominant step, as also justified in the ESI-Section S3. Moreover, since all dyes are studied under the same conditions, a linear relationship is observed between the values of k_1 and k_f , with a slope of $1.80 \pm 0.1 \text{ m}^{-1}$, representing the proportionality constant. This indicates the good agreement between the two mathematical approaches used in the kinetic study.

3.4. Isothermal study

In this section, we conducted studies on dyes 1, 7, 8, 12, 14, 18, and 21, particularly emphasizing dye 14, indigo carmine. This decision is well-founded due to its extensive usage in the textile industry, particularly in denim garments such as jeans and jackets. Due to its widespread application and demand within the fashion market, Indigo carmine holds significant sway, both environmentally and economically.

Hence, we carried out the isotherm study for this specific dye using both procedures detailed in the experimental section. We exclusively followed procedure B for the remaining dyes, maintaining a constant disk size while varying the dye concentration. Fig. 3 presents comprehensive results for dye 14, encompassing kinetic fittings (pseudo-first-order model and Crank-Dual model) and isotherm fittings conducted using the two distinct procedures: procedure A (with constant dye concentration while altering the F2 disk size) and procedure B (with a fixed F2 disk size while modifying the dye concentration). Analogous

figures for the other dyes examined (dyes 1, 7, 8, 12, 18, and 21) can be found in the ESI-Section S3 (Figures S7-S12).

In previous work, we have studied how the size and shape of adsorbates affect the adsorption process using this same type of material, which is highly relevant for understanding the differences observed between the various dyes in this study [42]. Among the dyes studied, only dye 14 conforms to a Freundlich isotherm. This compound differs from the rest because it exhibits a linear structure with charges at terminal groups. Due to this configuration, we believe it shows a preference for interaction with certain binding sites, causing the adsorbent surface to behave as a heterogeneous surface, where some sites exhibit more affinity for adsorption than others. The remaining dyes conform to the model of a favourable Langmuir isotherm (see ESI-Section S3, Figures S7e-S10e, S12e). Dye 12, likely due to its high k_1 resulting from its small size, the isotherm at a concentration of 50 mg L^{-1} could not be calculated.

Additionally, particular focus has been directed towards dye 14 due to its prevalent use in dyeing denim pants. Utilizing the isotherm data, the percentage of adsorption can be delineated concerning the ratio of grams of adsorbent to grams of dye (Fig. 3 f). Notably, it is discerned that with a ratio exceeding 25, removal surpasses 90 %.

3.5. Permeation study

The permeation curves analysis is reported in Fig. 4, and their parameter values are resumed in ESI-Section S4, Table S1. It can be seen that the time-lag, θ , for different dyes follows the order: $18 < 12 < 21 < 7 < 14$. An increase in θ indicates the steady-state flux is attained at longer times and, consequently, permeant affinity to the membrane follows the same order as θ . These results agree with the inverse order of the D values, which show the capacity of the molecules to pass through the membrane. In other words, considering the dye 14, it presents the highest affinity to the membrane but the lowest rate of diffusion, suggesting the greatest capacity of the membrane F2 to retain it. On the other hand, dyes 1 and 8 showed no measurable permeation after 14 days.

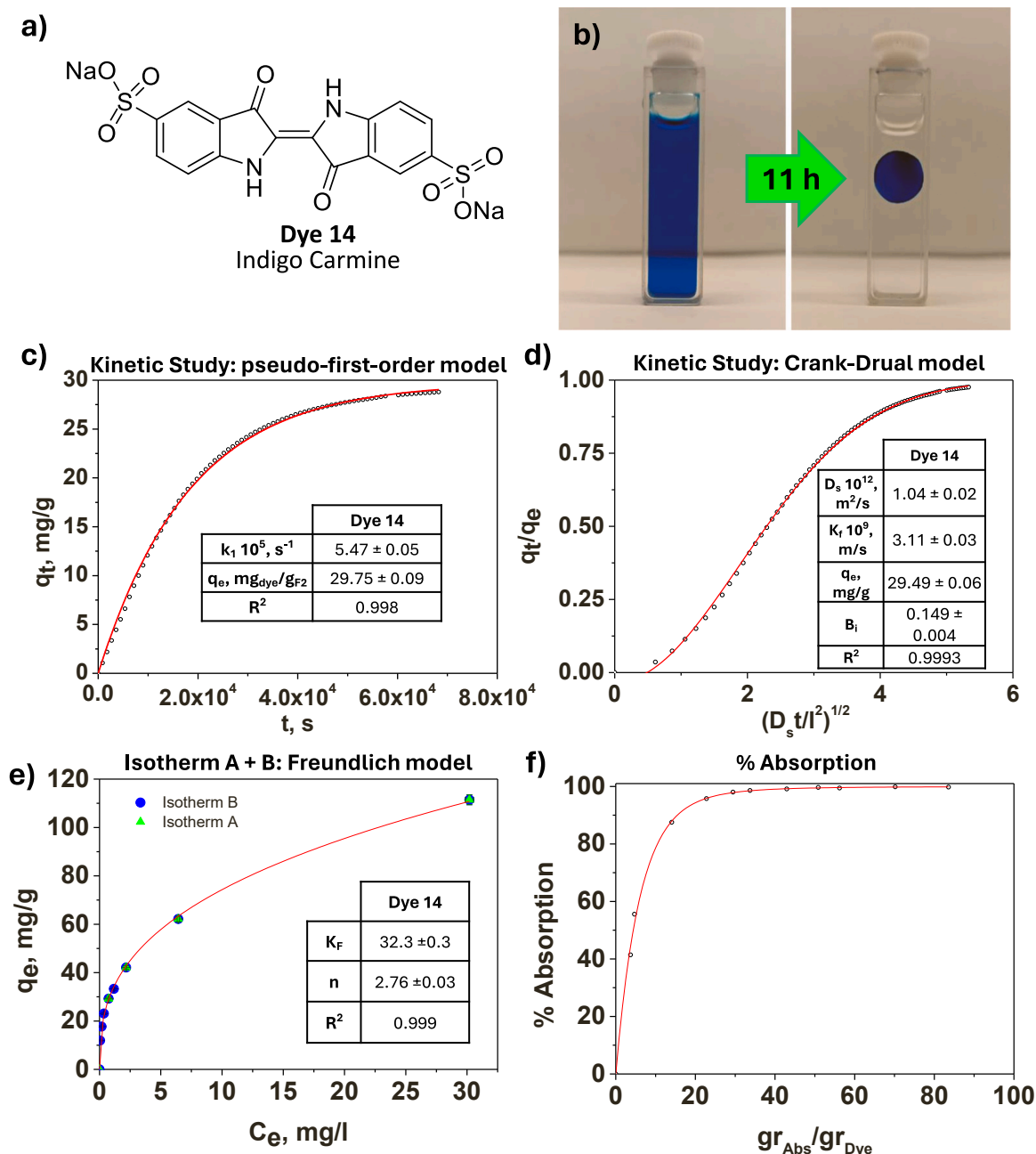


Fig. 3. a) Dye 14 chemical structure; b) Photograph of the initial dye solution (3.5 mL, 60 mg/L) before (left) and after (right) completion of the adsorption process using a 10 mm diameter disc of F2; c) kinetic study: pseudo-first-order model, λ_{abs} : 607 nm; d) kinetic study: Crank-Dual model, λ_{abs} : 607 nm; e) isotherm A + B: Freundlich model, λ_{abs} : 607 nm; f) Variation of the adsorption percentage of dye as a function of the ratio of gram of adsorbent to gram of dye.

3.6. Fluorescence analysis

It is worth noting that well-defined surfaces are obtained after permeation experiments. The surface in contact with the dye solution is colourful and shows a layer-like dye on the surface, which is not observable on the membrane side in contact with water. This allowed for a fluorescence study of the materials on both sides. Figure S13 (ESI-Section S5) shows that the membranes for each dye can present emission peaks and/or a shift of the peaks as function of the excited membrane side. In general, peaks with lower λ emission were observed when the side in contact with pure water was analysed (dashed line) than the λ observed for the side membrane in strict contact with the dye solution (solid line). These changes are noticeable for dyes 1, 8 and 14. In agreement, dye 14 showed the highest θ , P and K values in the

permeation analysis, which indicate the slowest rate of diffusion, higher rate of permeation and strongest affinity to the membrane. Moreover, this shift to higher λ_{emis} can also suggest that the dye molecule mainly interacts at the surface of the membranes. This finding aligns with the results obtained for isotherms, where it was deduced that adsorption primarily occurs on the material's surface.

3.7. Characterization of the interaction mechanism between dyes and F2

Due to the significance of Dye 14 in the textile industry, we conducted SEM experiments to characterize the interaction between Dye 14 and F2. Additionally, Dye 12 was included in this study because it is the only dye among those tested that contains an iron atom, which we considered particularly interesting for EDXS analysis of the samples.

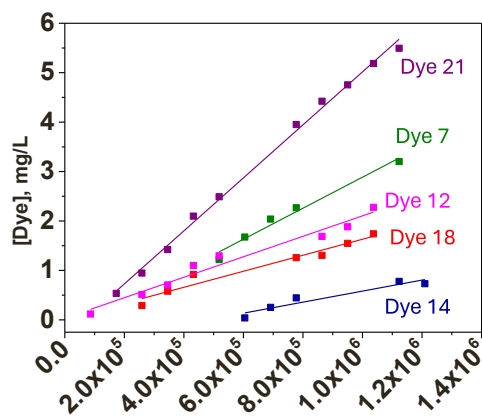


Fig. 4. Permeation analysis curves with dye 7 (green), dye 12 (magenta), dye 14 (blue), dye 18 (red) and dye 21 (purple). Analysis was performed at 25 °C, using a membrane thickness = 100 μm , area = 2 cm^2 , the content of beaker A = 200 mL of MQ water and content of beaker B = 200 mL of dye solution at 50 mg/L.

All materials used in this section were prepared by immersing a 10 mm diameter disc of F2 in 3.5 mL of a 50 ppm dye solution. In an initial experiment with Dye 12, we observed that our materials are not perfect and exhibit surface defects in the form of small holes (Fig. 5a). These defects are attributable to the imperfections in the glass moulds used during the preparation of these materials (Figure S1c). Interestingly, we noted that these defects could act as nucleation sites for the formation of Dye 12 crystals (Fig. 5b).

However, we do not believe that this is the initial process occurring during the adsorption of dyes on F2. In fact, our hypothesis posits that ion exchange occurs first [94], following a mechanism similar to that of ion exchange resins, as depicted graphically in the diagram in Fig. 5c. Following this initial process, a second process becomes apparent in the SEM images. Specifically, after the saturation of the active sites of the material, dye crystallization occurs on the surface of F2 rather than within the material, due to its dense nature (Fig. 5d).

In both the Dye 12 and Dye 14 experiments, nanoparticles and microparticles of the dye can be observed on the surface of the material. At this stage, the EDXS analysis of the Dye 12 particles was extremely informative, revealing high quantities of iron due to the organometallic nature of the dye, as shown in Fig. 5d.

To further our objective of characterizing the interaction between the dye and F2, we conducted PXRD experiments. The spectra shown in Fig. 5e display typical amorphous halos, which provide the average distance between polymer chains and allow us to observe the effect of chloride ion exchange with Dye 12 and Dye 14. This interchain distance is described by the equation $\langle R \rangle = 5/8(\lambda/\sin \theta_{\text{max}})$, indicating that as θ_{max} increases, the interchain distance decreases. When chloride ions are present between the chains, the distance is minimal due to chloride being the smallest anion (7.38 Å). Substituting this chloride with a larger anion, such as Dye 12 or Dye 14, significantly increases the interchain distance to 7.46 Å and 7.43 Å, respectively, resulting in a decrease in $2\theta_{\text{max}}$ from 15.00 to 14.84 and 14.89, respectively. These results also provide insights into how Dye 14 interacts with the material, as it is a much larger molecule than Dye 12 (Fig. 5g). However, both dyes produce nearly the same chain separation. In fact, the separation between chains with Dye 14 is slightly less. Our hypothesis is that the linear and elongated structure of Dye 14, along with the localization of two charges at the ends of the molecule, facilitates its alignment parallel to the polymeric chains, rather than transversely. Assuming this, the separation between chains would be less than that caused by Dye 12, as reflected in the molecular sizes shown in Fig. 5g and supported by the experimental results.

The results obtained from RAMAN experiments also confirmed the interaction between the dye and F2. Once again, the experiments with Dye 12 provided the highest quality information due to the intense band exhibited by Dye 12 at 2128 cm^{-1} . As shown in Fig. 5f, F2 does not exhibit any bands at these wavenumbers initially; however, after the adsorption process with Dye 12, it displays the characteristic band of the dye.

The ICP-MS results were also highly elucidative, particularly in justifying the ion exchange process. The F2 material initially had a chlorine concentration of 6906 ± 71 ppb, which decreased to 1166 ± 315 ppb and 2838 ± 373 ppb after the adsorption process of dyes 12 and 14, respectively. This indicates that the chlorides, which acted as counterions in the NNDA monomer, were released from the material and replaced by anionic dyes. Therefore, assuming the hypothesis that both dyes entered the three-dimensional network of the polymeric material, the concentration of Fe (in the case of Dye 12) and the concentration of S (in the case of Dye 14) should increase. Indeed, the results confirm this. The iron concentration increased from 53 ± 28 ppb in the original F2 to 4445 ± 27 ppb after the adsorption process of Dye 12. Similarly, the sulfur concentration increased from 43 ± 16 ppb in the original F2 to 4148 ± 527 ppb after the adsorption process of Dye 14 (ICP-MS data are means of 2 replicates \pm sd).

Regarding the total nitrogen measurement, this technique, like the others, confirmed the near-complete removal of both dyes (12 and 14) from the prepared solutions. In the experiment with Dye 12, the total nitrogen content decreased from 12.05 ± 0.10 ppm to 0.45 ± 0.02 ppm. In the experiment with Dye 14, the total nitrogen content dropped from $1.95 \text{ ppm} \pm 0.03$ to 0 (total nitrogen data are means of 3 replicates \pm sd).

The anionic exchange process that takes place results in the release of chloride anions into the water, which, at concentrations expected in realistic scenarios, pose no risk. Furthermore, the potential migration of substances from these materials (with non-significant modifications) into the water they are submerged in has already been studied in previous works [95], where tests were conducted according to the provisions of Commission Regulation (EU) No 10/2011 (and its amendments) concerning plastic materials and articles intended to come into contact with food, and the results were favourable.

3.8. Proof of concept

The proof of concept focused exclusively on dye 14. The main aim was to investigate potential interferences for domestic material use, specifically assessing whether fabric softeners and detergents affect the adsorption and kinetics of the material. Essentially, a kinetic assay using a 10 mm diameter disc of F2 was replicated by introducing standard quantities of detergent and fabric softener into the medium (3.5 mL of tap water, 10 μL of fabric softener, and 10 μL of detergent). After fitting the data to a pseudo-first-order model, the determined values for k_1 and q_e were $(5.8 \pm 0.1) \times 10^{-5} \text{ s}^{-1}$ and $5.75 \pm 0.03 \text{ mg/g}$, respectively. Comparable data were obtained in the assay without fabric softener or detergent ($(5.95 \pm 0.06) \times 10^{-5} \text{ s}^{-1}$ and $6.19 \pm 0.02 \text{ mg/g}$). Consequently, it can be inferred that typical quantities of fabric softener or detergent in a household washing machine do not impact the dye adsorption process.

Likewise, when analysing the results obtained for the Crank-Dual model in the presence of fabric softener or detergent, one observes values of D_s , k_f , q_e , and B_i as $(12.8 \pm 0.3) \times 10^{-13} \text{ m}^2/\text{s}$, $(2.86 \pm 0.08) \times 10^{-9} \text{ m/s}$, $5.78 \pm 0.03 \text{ mg/g}$, and 0.110 ± 0.006 , respectively. Similar results were obtained in the experiment conducted without fabric softener or detergent ($(9 \pm 3) \times 10^{-13} \text{ m}^2/\text{s}$, $(3.5 \pm 0.1) \times 10^{-9} \text{ m/s}$, $6.15 \pm 0.01 \text{ mg/g}$, and 0.21 ± 0.09). Like the pseudo-first-order model, it can be inferred that typical quantities of fabric softener or detergent in a household washing machine do not significantly influence the dye adsorption process when employing the Crank-Dual model.

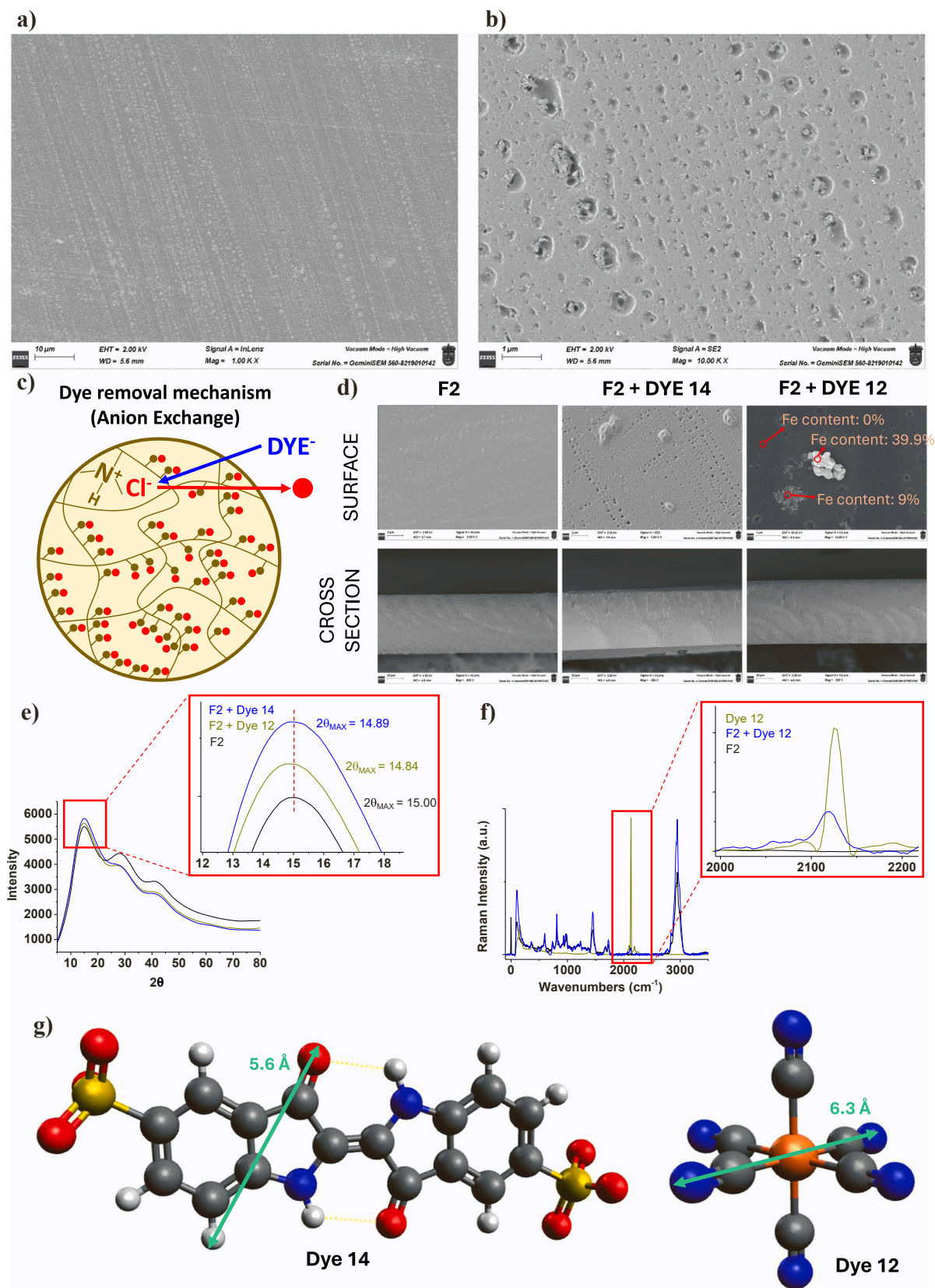


Fig. 5. Characterization of 10 mm diameter discs of F2, both before and after immersion in 3.5 mL of 50 ppm Dye 12 and Dye 14 solutions overnight. a) and b) SEM images of F2 + dye 12 (1000x and 10,000x magnification, respectively); c) diagram of the Ion Exchange Mechanism Underpinning Dye Removal Using F2; d) SEM images of F2, F2 + dye 12 and F2 + dye 14 (surface and cross-section); e) PXRD spectra of F2, F2 + dye 12 and F2 + dye 14 showing $2\theta_{MAX}$; f) RAMAN spectra of F2, dye 12 and F2 + dye 12; g) The molecular sizes of dyes 12 and 14.

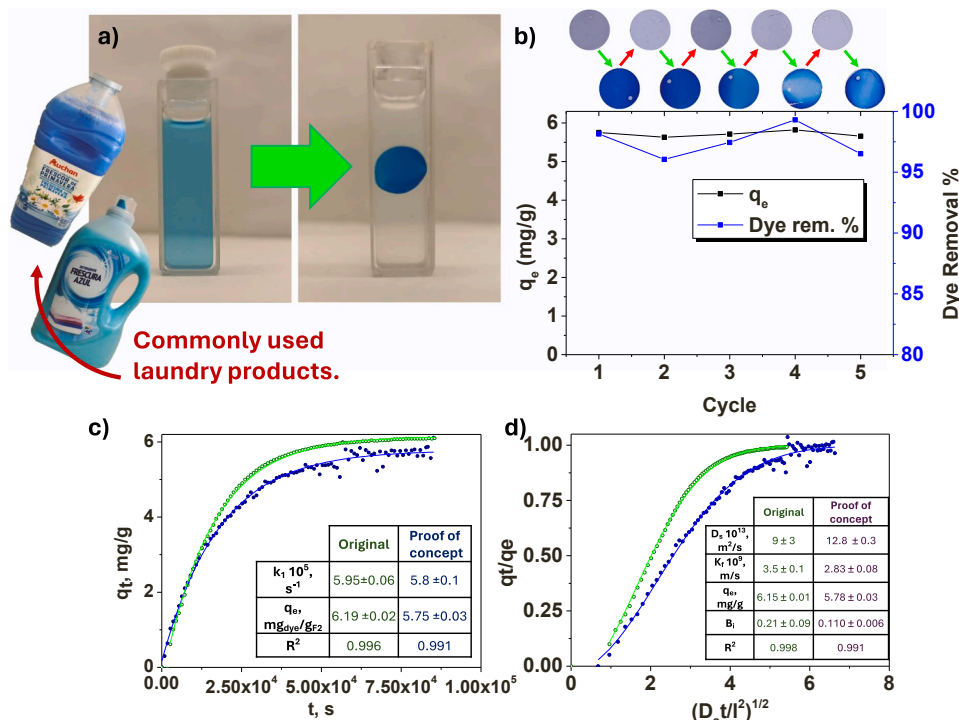


Fig. 6. a) Initial dye solution at 10 mg/L (left) and after the completion of the adsorption process (right), conducted using a 10 mm diameter F2 disk, in the presence of 10 mL detergent and 10 mL fabric softener in tap water (3.5 mL). b) Reuse of a 10 mm diameter F2 disk. The graph depicts the absorbance of a 10 mg/L dye 14 solution in distilled water (3.5 mL) before and after introducing the F2 disk. Following the adsorption process, the disk is washed with a 1 mol/L aqueous solution of NaOH for 12 h, renewing the washing solution twice. Subsequently, it is reprotonated with a 4 % HCl solution, and the adsorption process is initiated again. This process was repeated 5 times. Kinetic study of the adsorption of dye 14 using a 10 mm F2 disk, fitting the pseudo-first-order (c) and Crank-Dual (d) models. The study in distilled water is represented in green, while the study in tap water with detergent and fabric softener is represented in blue.

In the graphs of Fig. 6, it can be observed that the trend remains consistent both with and without detergents. Although the presence of detergents introduces some dispersion in the measurements, especially in the later points of the kinetics, the values of the constants were examined (Figs. 4c and 4d), and considering the error, no significant differences were found between the calculated parameters in both processes. Therefore, it can be concluded that the adsorption capacities of the material are not affected by the presence of co-formulants in commercial detergents and fabric softener formulations.

3.9. Reusability study

The reusability of this material relies on the *N,N*-dimethylamino functional group contained in the NNDA monomer, which has a theoretical pKa of approximately 8. In fact, the material is only capable of interacting with anionic dyes when it has been previously protonated, and the pH of the medium is below 8. Under these conditions, the *N,N*-dimethylamino functional group contained in the NNDA monomer is protonated, thus possessing a formal positive charge and a chloride counteranion. This chloride anion can be exchanged for molecules of anionic dyes. However, if after adsorption the material is placed in an basic aqueous medium, the *N,N*-dimethylamino functional group deprotonates, loses its positive charge, and therefore, the electrostatic interaction with the anionic dye disappears, leading to the release of the dye into the medium.

Thus, the material was subjected to 5 cycles of adsorption/desorption, maintaining its properties and adsorption capacity throughout. Fig. 6b illustrates absorbance graphs of dye solutions before and after adsorption, accompanied by corresponding images of the material taken before adsorption and after desorption. These data demonstrate consistent performance of the material across all cycles.

Furthermore, the desorption process damages neither the material nor the dye, which is recovered in an aqueous solution form as a sodium salt. Much of this merit lies in its dense (non-porous) nature, which withstands the stress exerted on the material during these cycles, enabling its recovery and reuse. Considering that in the textile industry, 10 % of the dyes used are discharged with wastewater [2], these reusability properties represent an outstanding advantage from an industrial and environmental point of view. Herein, the reuse of dyes would lower their costs and applied amount, with a reduced environmental impact by decreasing contamination.

3.10. Comparative study

The contamination by dyes is a real problem. While the literature provides numerous materials capable of extracting dyes from aqueous media (see Table 3), most of these methods present certain inconveniences or disadvantages. These drawbacks include being non-reusable [13,14,16,17,20,21,96], specific to a single dye [12–14, 16–20,23], causing dye degradation [13,14,18–21], requiring UV light for operation or performance enhancement [13,16,18,21,90], or being contingent on specific conditions such as phytoremediation [2], which, while initially a sustainable alternative, depends on plants growing time and conditions as well as big implant space. The alternative proposed in this study does not exhibit any of these disadvantages. Firstly, the material can be synthesized using low-cost commercial reagents. It does not require UV light for operation or performance improvement. While not biodegradable, its reusability cycles allow for both material reutilization and the recovery of 100 % of the adsorbed dye. Additionally, it can be employed for more than 20 different dyes. The material remains unaffected by laundry soaps, enabling its use in both industrial and domestic settings.

Table 3

Comparative study of materials for dye extraction: analysis based on material type, dye removal efficiency, specific dyes utilized, and material reusability.

Technique/Process	Material	Dye removal (%)	Dye	Reusability of the material	Ref
Ultrafiltration membrane	Polyamide + Cetyl(hexadecyl) pyridinium chloride	73.50	Eosin	Yes	[12]
	Polysulfone + Titanium dioxide	97.00	Eosin Yellow	No	[13]
	Polyvinyl alcohol + Zeoliticimidazole framework (ZIF-8)/chitosan	84.55	Malachite Green (MG)	No	[14]
	Cellulose + Graphene oxide	> 90.00	Victoria blue B, Methyl Violet 2B, Rhodamine6G	Probably*	[15]
Ion exchange	Polysulfone+ Sulfated nano-titania	90.40	Methylene blue (MB)	No	[16]
	Chitosan + Carboxylated MWCNTs	80.00–90.00	MB, Methyl orange (MO)	No	[17]
	Polysulfone poly + (N-vinylcaprolactam-TiO ₂ -acrylic acid)	93.70	MB	Partially	[18]
	Micro-sized ammonium phosphomolybdate (APM)	94.6	MB, MG, Methyl Red (MR)	Yes	[90]
Electrocoagulation	Anode Fe	96.11	Brilliant green	Yes	[19]
Advanced oxidation process	H ₂ O ₂ , and Fe ²⁺	98.35	Acid Violet 49	No	[96]
Photocatalytic degradation	ZnO	97.25	Acid Red 88	No	[21]
		80	MB		
Coagulation and flocculation	Moringa oleifera Lam (MO) seeds and subsequently ultrafiltration (UF) in TiO ₂ -modified membranes	100	Black 5	No	[20]
Phytoremediation	<i>Tagetes</i>	59	Textile dye (no specific)	Yes	[2]
	<i>Aster amellus</i>	50			
	<i>Portulaca grandiflora patula</i>	46			
	<i>Gaillardia grandiflora</i>	73			
Adsorption	Multiwall carbon nanotubes	98.7	Acid Scarlet 3 R	Yes	[22]
		97.2	Auramine O		
		97.6	Basic Violet 2B crystal		
	Sol-gel immobilized polyurethane foams (sol-gel/PUF)	90.0–100	Eosin yellow	Yes	[23]
This work	> 90 %	More than 20 dyes	Yes		

*The authors explain that this type of material is reusable, but they do not specifically study it in the article.

4. Conclusions

In this work, we developed a novel smart polymer to address the escalating environmental threat posed by industrial waste and the significant volume of synthetic dyes discharged into water bodies. We successfully designed and prepared a reusable polyacrylic film with remarkable efficiency in capturing a diverse spectrum of families of textile dyes. The polymeric film exhibits specific interactions with dyes extracting and colouring the material. The textile dye removal efficiency of the film was high (up to >90 % dye removal efficiency) for anionic-state dyes at the working conditions with external diffusion being the dominant factor influencing the process rate, as the adsorption of the dye occurs on the material's surface. Moreover, the presence of fabric detergent and softener does not affect the material adsorption capacity. Unlike other materials prepared for similar purposes, this membrane showed durability, enhanced manageability, and good mechanical and thermal properties, providing a practical solution for water dye decontamination. These properties, including its ability to minimize waste generation through reusability (at least 5 cycles of adsorption/desorption), and the capability of recovering 100 % of the adsorbed dye, make it highly suitable for practical applications in both industrial and domestic settings, accessible even to non-specialists. Its versatility extends to accommodating over 20 different dye types, while remaining unaffected by laundry detergents, further enhancing its usability. The study's findings hold promise for significantly mitigating water pollution stemming from synthetic dyes, offering a comprehensive and sustainable solution that addresses both environmental concerns and practical usability. This inclusive approach, encompassing various dye types commonly employed in the textile industry, underscores the material's adaptability and potential for widespread use in diverse industrial and household settings. Further research and development in this area could lead to broader adoption of such innovative materials, fostering sustainability in pollution management practices on a global scale.

Environmental implication

Dyes released during laundry processes should be classified as "hazardous materials" owing to their significant toxicity towards aquatic

organisms, with the potential to disrupt ecosystems and harm aquatic biodiversity. This paper discusses the development of a novel acrylic material in film form, engineered to extract toxic anionic dyes. This study directly contributes to mitigating the environmental impact associated with the fashion industry and the domestic use of textiles. It can be implemented on both an industrial and personal scale, thereby encouraging more sustainable practices and promoting collaborative citizen science efforts towards

Declaration of Competing Interest

The authors declare that they have no known competing financial interests or personal relationships that could have appeared to influence the work reported in this paper.

Data availability

No data was used for the research described in the article.

Acknowledgments

We gratefully acknowledge the financial support provided by all funders. This work was supported by the Regional Government of Castilla y León (Junta de Castilla y León) and by the Ministry of Science and Innovation MICIN and the European Union NextGenerationEU PRTR. Author Saul Vallejos received grant BG22/00086 funded by Spanish Ministerio de Universidades. Author Marta Guembe-García received funding from the Spanish Ministerio de Universidades-European Union under the framework of NextGeneration EU RD 289/2021 for her Post-Doc position. Author Jose Miguel García received grant PID2020-113264RB-I00 funded by MCIN/AEI/ 10.13039/501100011033 and by "ERDF A way of making Europe", and grant TED2021-129419B-C21 funded by MCIN/AEI/ 10.13039/501100011033 and by the "European Union NextGenerationEU/PRTR". The financial support provided by Fondo Europeo de Desarrollo Regional-European Regional Development Fund (FEDER, ERDF) and Regional Government of Castilla y León -Consejería de Educación, Junta de Castilla y León- (BU025P23) is gratefully acknowledged. Artur Valente and Gianluca Utzeri thank the

financial support from The Coimbra Chemistry Centre through Projects UIDB/00313/2020 and UIDP/00313/2020 (FCT).

Supplementary material

Materials; characterization of the material; adsorption of dyes: more information about the kinetic, isotherm, and fluorescence study; and permeation study.

Open data

Open Data is available at <https://riubu.ubu.es/handle/10259/5684> under the name "UBU-Polymers Research Group 13022024".

Appendix A. Supporting information

Supplementary data associated with this article can be found in the online version at [doi:10.1016/j.jhazmat.2024.135006](https://doi.org/10.1016/j.jhazmat.2024.135006).

References

- Cao, D., Niu, K., Yu, F., 2011. Economic analysis on pollution control for textile industry. *Adv Mater Res* 332–334, 1087–1092. <https://doi.org/10.4028/WWW.SCIENTIFIC.NET/AMR.332-334.1087>.
- Chandanshive, V.V., Kadam, S.K., Khandare, R.V., Kurade, M.B., Jeon, B.H., Jadhav, J.P., et al., 2018. In situ phytoremediation of dyes from textile wastewater using garden ornamental plants, effect on soil quality and plant growth. *Chemosphere* 210, 968–976. <https://doi.org/10.1016/j.chemosphere.2018.07.064>.
- Ulson de Souza, S.M.A.G., Forgiarini, E., Ulson de Souza, A.A., 2007. Toxicity of textile dyes and their degradation by the enzyme horseradish peroxidase (HRP). *J Hazard Mater* 147, 1073–1078. <https://doi.org/10.1016/J.JHAZMAT.2007.06.003>.
- Al-Tohamy, R., Ali, S.S., Li, F., Okasha, K.M., Mahmoud, Y.A.G., Elsamahy, T., et al., 2022. A critical review on the treatment of dye-containing wastewater: ecotoxicological and health concerns of textile dyes and possible remediation approaches for environmental safety. *Ecotoxicol Environ Saf* 231, 113160. <https://doi.org/10.1016/J.ECOENV.2021.113160>.
- M. Hassan, C.C.- Chemosphere, undefined 2018, A critical review on recent advancements of the removal of reactive dyes from dyehouse effluent by ion-exchange adsorbents, ElsevierMM Hassan, C. CarrChemosphere, 2018•Elsevier (n. d.).
- Imran, M., Crowley, D.E., Khalid, A., Hussain, S., Mumtaz, M.W., Arshad, M., 2015. Microbial biotechnology for decolorization of textile wastewaters. *Rev Environ Sci Biotechnol* 14, 73–92. <https://doi.org/10.1007/S11157-014-9344-4>.
- Lellis, B., Fávoro-Polonio, C.Z., Pamphile, J.A., Polonio, J.C., 2019. Effects of textile dyes on health and the environment and bioremediation potential of living organisms. *Biotechnol Res Innov* 3, 275–290. <https://doi.org/10.1016/J.BIORL.2019.09.001>.
- Maheshwari, K., Agrawal, M., Gupta, A.B., 2021. Dye Pollut Water Wastewater BT - Nov Mater Dye-Contain Wastewater Treat.
- Clark, M., 2011. *Handb Text Ind dyeing: Princ, Process Types Dyes*.
- Christie, R., 2007. *Environ Asp Text dyeing*. <https://doi.org/10.1533/9781845693091>.
- Hunger, K., 2007. *Ind dyes: Chem, Prop, Appl*.
- Purkait, M.K., DasGupta, S., De, S., 2004. Removal of dye from wastewater using micellar-enhanced ultrafiltration and recovery of surfactant. *Sep Purif Technol* 37, 81–92. <https://doi.org/10.1016/j.seppur.2003.08.005>.
- Kuvarega, A.T., Khumalo, N., Dlamini, D., Mamba, B.B., 2018. Polysulfone/N,Pd co-doped TiO₂ composite membranes for photocatalytic dye degradation. *Sep Purif Technol* 191, 122–133. <https://doi.org/10.1016/j.seppur.2017.07.064>.
- Khajavian, M., Salehi, E., Vatanpour, V., 2020. Chitosan/polyvinyl alcohol thin membrane adsorbents modified with zeolitic imidazolate framework (ZIF-8) nanostructures: batch adsorption and optimization. *Sep Purif Technol* 241, 116759. <https://doi.org/10.1016/j.seppur.2020.116759>.
- Liu, P., Zhu, C., Mathew, A.P., 2019. Mechanically robust high flux graphene oxide - nanocellulose membranes for dye removal from water. *J Hazard Mater* 371, 484–493. <https://doi.org/10.1016/j.jhazmat.2019.03.009>.
- Pereira, V.R., Isloor, A.M., Bhat, U.K., Ismail, A.F., Obaid, A., Fun, H.K., 2015. Preparation and performance studies of polysulfone-sulfated nano-titania (S-TiO₂) nanofiltration membranes for dye removal. *RSC Adv* 5, 53874–53885. <https://doi.org/10.1039/c5ra07994b>.
- Shi, J., Wu, T., Teng, K., Wang, W., Shan, M., Xu, Z., et al., 2016. Simultaneous electrospinning and spraying toward branch-like nanofibrous membranes functionalised with carboxylated MWCNTs for dye removal. *Mater Lett* 166, 26–29. <https://doi.org/10.1016/j.matlet.2015.12.024>.
- Singh, R., Sinha, M.K., Purkait, M.K., 2020. Stimuli responsive mixed matrix polysulfone ultrafiltration membrane for humic acid and photocatalytic dye removal applications. *Sep Purif Technol* 250, 117247. <https://doi.org/10.1016/j.seppur.2020.117247>.
- Mariah, G.K., Pak, K.S., 2020. Removal of brilliant green dye from aqueous solution by electrocoagulation using response surface methodology. *Mater Today Proc* 20, 488–492. <https://doi.org/10.1016/j.matpr.2019.09.175>.
- Beluci, N. de C.L., Mateus, G.A.P., Miyashiro, C.S., Homem, N.C., Gomes, R.G., Fagundes-Klen, M.R., et al., 2019. Hybrid treatment of coagulation/flocculation process followed by ultrafiltration in TIO 2 -modified membranes to improve the removal of reactive black 5 dye. *Sci Total Environ* 664, 222–229. <https://doi.org/10.1016/j.scitotenv.2019.01.199>.
- Tabrizi Hafez Moghaddas, S.M., Elahi, B., Javanbakht, V., 2020. Biosynthesis of pure zinc oxide nanoparticles using Quince seed mucilage for photocatalytic dye degradation. *J Alloy Compd* 821, 153519. <https://doi.org/10.1016/j.jallcom.2019.153519>.
- Shabaan, O.A., Jahin, H.S., Mohamed, G.G., 2020. Removal of anionic and cationic dyes from wastewater by adsorption using multiwall carbon nanotubes. *Arab J Chem* 13, 4797–4810. <https://doi.org/10.1016/j.arabjc.2020.01.010>.
- Ghandourah, M.A., Orif, M.I., Al-Farawati, R.K., El-Shahawi, M.S., Abu-Zied, R.H., 2023. Sol-Gel functionalized polyurethane foam-packed mini-column as an efficient solid extractor for the rapid and ultra-trace detection of textile dyes in water. *Gels* 9, 1–13. <https://doi.org/10.3390/gels9110884>.
- Pandey, S., Makhado, E., Kim, S., Kang, M., 2023. Recent developments of polysaccharide based superabsorbent nanocomposite for organic dye contamination removal from wastewater — A review. *Environ Res* 217, 114909. <https://doi.org/10.1016/j.envres.2022.114909>.
- Ibrahim, I.M., Radwan, M.A., Sadek, M.A., Darwish, S.A., Mostafa, N.Y., 2023. Effect of electrostatic interactions on the dye removal behavior of different hydrogel based materials. *Egypt J Chem* 66, 257–261. <https://doi.org/10.21608/EJCHEM.2022.176630.7228>.
- Bhattacharya, S., Shunmugam, R., 2020. Polymer based gels and their applications in remediation of dyes from textile effluents. *J Macromol Sci Part A* 57, 906–926. <https://doi.org/10.1080/10601325.2020.1782229>.
- Ruan, C., Ma, Y., Shi, G., He, C., Du, C., Jin, X., et al., 2022. Self-assembly cellulose nanocrystals/SiO₂ composite aerogel under freeze-drying: adsorption towards dye contaminant. *Appl Surf Sci* 592, 153280. <https://doi.org/10.1016/J.APSUSC.2022.153280>.
- Utzeri, G., Guirado-Moreno, J.C., Cova, T.F.G.G., Pais, A.A.A.C., De Carvalho, L.A. E.B., Ibeas, S., et al., 2024. Reusable and effective polyacrylic membranes for mecoprop and bentazon extraction. *NPJ Clean Water* 7. <https://doi.org/10.1038/s41545-024-00328-3>.
- A.N. Alsulami, A.S. Alharthi, F.M. Alshareef, H. Alwael, E.A. Bahaidarah, M. Ouban, C. Ma, Y., Shi, G., He, C., Du, C., Jin, X., et al., 2022. Self-assembly cellulose nanocrystals/SiO₂ composite aerogel under freeze-drying: adsorption towards dye contaminant. *Appl Surf Sci* 592, 153280. <https://doi.org/10.1016/J.APSUSC.2022.153280>.
- Pandey, S., Son, N., Kang, M., 2022. Synergistic sorption performance of karaya gum crosslink poly(acrylamide-co-acrylonitrile) @ metal nanoparticle for organic pollutants. *Int J Biol Macromol* 210, 300–314. <https://doi.org/10.1016/J.IJBIOMAC.2022.05.019>.
- Makhado, E., Motshabi, B.R., Allouss, D., Ramohlola, K.E., Modibane, K.D., Hato, M.J., et al., 2022. Development of a ghatti gum/poly (acrylic acid)/TiO₂ hydrogel nanocomposite for malachite green adsorption from aqueous media: statistical optimization using response surface methodology. *Chemosphere* 306, 135524. <https://doi.org/10.1016/J.CHEMOSPHERE.2022.135524>.
- Bhattacharya, S., Shunmugam, R., 2020. Polymer based gels and their applications in remediation of dyes from textile effluents. *J Macromol Sci Part A* 57, 906–926. <https://doi.org/10.1080/10601325.2020.1782229>.
- Zhu, H., Chen, S., Luo, Y., 2023. Adsorption mechanisms of hydrogels for heavy metal and organic dyes removal: a short review. *J Agric Food Res* 12, 100552. <https://doi.org/10.1016/J.JAFR.2023.100552>.
- Hu, X.S., Liang, R., Sun, G., 2018. Super-adsorbent hydrogel for removal of methylene blue dye from aqueous solution. *J Mater Chem A* 6, 17612–17624. <https://doi.org/10.1039/C8TA04722G>.
- Shalla, A.H., Bhat, M.A., Yaseen, Z., 2018. Hydrogels for removal of recalcitrant organic dyes: a conceptual overview. *J Environ Chem Eng* 6, 5938–5949. <https://doi.org/10.1016/J.JECE.2018.08.063>.
- Vallejos, S., Muñoz, A., García, F.C., Serna, F., Ibeas, S., García, J.M., 2012. Methacrylate copolymers with pendant piperazinedione-sensing motifs as fluorescent chemosensory materials for the detection of Cr(VI) in aqueous media. *J Hazard Mater* 227–228, 480–483. <https://doi.org/10.1016/j.jhazmat.2012.05.047>.
- Pascual, B.S., Vallejos, S., Reglero Ruiz, J.A., Bertolín, J.C., Represa, C., García, F. C., et al., 2019. Easy and inexpensive method for the visual and electronic detection of oxidants in air by using vinyllic films with embedded aniline. *J Hazard Mater* 364, 238–243. <https://doi.org/10.1016/j.jhazmat.2018.10.039>.
- Vallejos, S., Muñoz, A., Ibeas, S., Serna, F., García, F.C., García, J.M., 2014. Selective and sensitive detection of aluminium ions in water via fluorescence “turn-on” with both solid and water soluble sensory polymer substrates. *J Hazard Mater* 276, 52–57. <https://doi.org/10.1016/j.jhazmat.2014.05.017>.
- Bustamante, S.E., Vallejos, S., Pascual-Portal, B.S., Muñoz, A., Mendia, A., Rivas, B. L., et al., 2019. Polymer films containing chemically anchored diazonium salts with long-term stability as colorimetric sensors. *J Hazard Mater* 365, 725–732. <https://doi.org/10.1016/j.jhazmat.2018.11.066>.
- García Pérez, J.M., García García, F.C., Vallejos, S., Trigo, M., Reglero-Ruiz, J.A., 2022. Smart polymers. Principles and Applications. De Gruyter, Boston. <https://doi.org/10.1515/9781501522468>.
- Vallejos, S., Muñoz, A., Ibeas, S., Serna, F., García, F.C., García, J.M., 2013. Solid sensory polymer substrates for the quantification of iron in blood, wine and water

- by a scalable RGB technique. *J Mater Chem A* 1, 15435–15441. <https://doi.org/10.1039/c3ta12703f>.
- [42] Guembe-García, M., Peredo-Guzmán, P.D., Santaolalla-García, V., Moradillo-Renuncio, N., Ibeas, S., Mendía, A., et al., 2020. Why is the sensory response of organic probes within a polymer film different in solution and in the solid-state? Evidence and application to the detection of amino acids in human chronic wounds. *Polym (Basel)* 12. <https://doi.org/10.3390/POLYM12061249>.
- [43] Do, D.D., 1998. Adsorption analysis: equilibria and kinetics. *Chem Eng* 2, 913.
- [44] Langmuir, I., 1918. The adsorption of gases on plane surfaces of glass, mica and platinum. *J Am Chem Soc* 40, 1361–1403. <https://doi.org/10.1021/JA02242A004/ASSET/JA02242A004.FP.PNG.V03>.
- [45] Freundlich, H., 1907. Over the adsorption in solution. *J Phys Chem* 57U, 385–470. <https://doi.org/10.1515/ZPCH-1907-5723/HTML>.
- [46] Valente, A.J.M., Polishchuk, A.Y., Lobo, V.M.M., Burrows, H.D., 2000. Transport properties of concentrated aqueous sodium dodecyl sulfate solutions in polymer membranes derived from cellulose esters. *Langmuir* 16, 6475–6479. <https://doi.org/10.1021/LA000286L/ASSET/IMAGES/MEDIUM/LA000286LE000006.GIF>.
- [47] Yadav, H.K.S., Raizaday, A., 2016. Inorganic nanobiomaterials for medical imaging. *Nanobiomater Med Imaging Appl Nanobiomater* 365–401. <https://doi.org/10.1016/B978-0-323-41736-5.00012-1>.
- [48] Tuzimski, T., 2015. Advanced spectroscopic detectors for identification and quantification. UV-Visible, Fluorescence, Infrared Spectroscopy, Instrum Thin-Layer Chromatogr 239–248. <https://doi.org/10.1016/B978-0-12-417223-4.00009-1>.
- [49] Niwa, M., 2019. Derivatization and labeling techniques. *Encycl Anal Sci* 210–213. <https://doi.org/10.1016/B978-0-12-409547-2.13970-8>.
- [50] Myers, D.N., 2019. Innovations in monitoring with water-quality sensors with case studies on floods, hurricanes, and harmful algal blooms. *Sep Sci Technol* 11, 219–283. <https://doi.org/10.1016/B978-0-12-815730-5.00010-7>.
- [51] Christie, R.M., 2011. Fluorescent dyes. *Handb Text Ind Dye Princ Process Types Dye* 1, 562–587. <https://doi.org/10.1533/9780857093974.2.562>.
- [52] Singh, V., Lalitha, K., Maheswari, C.U., Sridharan, V., Pradhan, D., Batra, S., et al., 2024. Remediation of dyes using supramolecular material derived from carbohydrate based π -gelator using the bottom-up assembly approach. *ACS Omega* 9, 5695–5704. <https://doi.org/10.1021/ACSOMEGA.3C08179/ASSET/IMAGES/LARGE/AO3C08179.0007.JPEG>.
- [53] Pablos, J.L., Vallejos, S., Ibeas, S., Muñoz, A., Serna, F., García, F.C., et al., 2015. Acrylic polymers with pendant phenylboronic acid moieties as “turn-off” and “turn-on” fluorescence solid sensors for detection of dopamine, glucose, and fructose in water. *ACS Macro Lett* 4, 979–983. https://doi.org/10.1021/ACSMACROLETT.5B00465/SUPPL_FILE/MZ5B00465_SI_001.PDF.
- [54] Guirado-Moreno, J.C., Carreira-Barral, I., Ibeas, S., García, J.M., Granès, D., Marchet, N., et al., 2023. Democratization of copper analysis in grape must following a polymer-based lab-on-a-chip approach. *ACS Appl Mater Interfaces* 15, 16055–16062. <https://doi.org/10.1021/ACSAMI.3C00395>.
- [55] Vallejo-García, J.L., Arnaiz, A., Busto, M.D., García, J.M., Vallejos, S., 2023. Film-shaped reusable smart polymer to produce lactose-free milk by simple immersion. *Eur Polym J* 200, 112495. <https://doi.org/10.1016/J.EURPOLYMJ.2023.112495>.
- [56] Mordant Blue 29 | C23H13Cl2Na3O9S | CID 54682456 - PubChem, (n.d.).
- [57] Pytlakowska, K., Zerzucha, P., Czoik, R., 2011. Influence of mixed cationic-anionic surfactant systems on the spectral properties of C.I. Mordant Blue 29 and its complexes with Iron(III). *Anal Sci* 27, 555–560. <https://doi.org/10.2116/ansalsci.27.555>.
- [58] Mordant Blue 3 | 3564–18–9, (n.d.).
- [59] Fagan, C., Kiernan, J.A., 2020. Certification procedures used by the biological stain commission for eriochrome cyanine R (C.I. 43820, Mordant blue 3). *Biotech Histochem* 95, 396–402. <https://doi.org/10.1080/10520295.2020.1748229>.
- [60] Poulos, I., Micropoulou, E., Panou, R., Kostopoulou, E., 2003. Photooxidation of eosin Y in the presence of semiconducting oxides. *Appl Catal B Environ* 41, 345–355. [https://doi.org/10.1016/S0926-3373\(02\)00160-1](https://doi.org/10.1016/S0926-3373(02)00160-1).
- [61] HanOfAcilnd, (n.d.).
- [62] Christie, R.M., 2011. Fluorescent dyes. in: *Handb. Text. Ind. Dye*. Elsevier, pp. 562–587. <https://doi.org/10.1533/9780857093974.2.562>.
- [63] Kumar, A., Raorane, C.J., Syed, A., Bahkali, A.H., Elgorban, A.M., Raj, V., et al., 2023. Synthesis of TiO₂, TiO₂/PANI, TiO₂/PANI/GO nanocomposites and photodegradation of anionic dyes Rose Bengal and thymol blue in visible light. *Environ Res* 216, 114741. <https://doi.org/10.1016/J.ENVRES.2022.114741>.
- [64] Reshetnyak, E.A., Rysukhina, A.I., Kameeva, N.N., Goloviznina, K.V., 2017. Influence of tetrabutylammonium bromide and sodium bromide on acid-base properties of thymol blue in water-ethanol medium. *Period Karazin Ua* 29, 46–52. <https://doi.org/10.26565/2220-637X-2017-29-04>.
- [65] Skjold, L.M., Jørgensen, L. v G., Dyhr, K.S., Köppl, C.J., McKnight, U.S., Bauer-Gottwein, P., et al., 2021. Assessing the aquatic toxicity and environmental safety of tracer compounds Rhodamine B and Rhodamine WT. *Water Res* 197, 117109. <https://doi.org/10.1016/J.WATRES.2021.117109>.
- [66] Zamouche, M., Hamdaoui, O., 2012. Sorption of Rhodamine B by Cedar Cone: effect of Ph and ionic strength. *Energy Procedia* 18, 1228–1239. <https://doi.org/10.1016/J.EGYPRO.2012.05.138>.
- [67] EPA, 2019. Provisional peer reviewed toxicity values for acenaphthylene. *Public Health*.
- [68] Sabnis, R.W., 2010. *Handbook of biological dyes and stains: Synthesis and industrial applications*. John Wiley & Sons.
- [69] Siddiqui, S.I., Allehyani, E.S., Al-Harbi, S.A., Hasan, Z., Abomuti, M.A., Rajor, H.K., et al., 2023. Investigation of congo red toxicity towards different living organisms: a review. *Processes* 11, 807. <https://doi.org/10.3390/pr11030807>.
- [70] Thioflavin T | C17H19ClN2S | CID 16953 - PubChem, (n.d.).
- [71] MolGpKa, (n.d.).
- [72] Vyavahare, G., Gurav, R., Patil, R., Sutar, S., Jadhav, P., Patil, D., et al., 2021. Sorption of brilliant green dye using soybean straw-derived biochar: characterization, kinetics, thermodynamics and toxicity studies. *Environ Geochem Health* 43, 2913–2926. <https://doi.org/10.1007/S10653-020-00804-Y/FIGURES/6>.
- [73] Abbas, M., 2020. Removal of brilliant green (BG) by activated carbon derived from medlar nucleus (ACMN) – Kinetic, isotherms and thermodynamic aspects of adsorption. *Adsorpt Sci Technol* 38, 464–482. https://doi.org/10.1177/0263617420957829/ASSET/IMAGES/LARGE/10.1177_0263617420957829-FIG9.JPEG.
- [74] Pearce, J., 1994. Studies of any toxicological effects of Prussian blue compounds in mammals—A review. *Food Chem Toxicol* 32, 577–582. [https://doi.org/10.1016/0278-6915\(94\)90116-3](https://doi.org/10.1016/0278-6915(94)90116-3).
- [75] Steingruber, E., 2004. Indigo and indigo colorants. *Ullmann's Encycl Ind Chem*. https://doi.org/10.1002/14356007.A14_149.PUB2.
- [76] Ristea, M.E., Zarnescu, O., 2023. Indigo carmine: between necessity and concern. *J Xenobiotics* 13, 509–528. <https://doi.org/10.3390/jox13030033>.
- [77] Malik, P.K., 2003. Use of activated carbons prepared from sawdust and rice-husk for adsorption of acid dyes: a case study of Acid Yellow 36. *Dye Pigment* 56, 239–249. [https://doi.org/10.1016/S0143-7208\(02\)00159-6](https://doi.org/10.1016/S0143-7208(02)00159-6).
- [78] Bistas, E., Sanghavi, D.K., 2023. Methylene Blue. *Hist Mod Clin Toxicol* 231–241. <https://doi.org/10.1016/B978-0-12-822218-8.00052-1>.
- [79] Sousa, H.R., Silva, L.S., Sousa, P.A.A., Sousa, R.R.M., Fonseca, M.G., Osajima, J.A., et al., 2019. Evaluation of methylene blue removal by plasma activated pylygorskites. *J Mater Res Technol* 8, 5432–5442. <https://doi.org/10.1016/J.JMRT.2019.09.011>.
- [80] Merck KGaA, Pinacyanol chloride, (n.d.).
- [81] Shapovalov, S.A., 2022. The first century of successful applications of pinacyanol: some noteworthy results. *Colorants* 1, 165–192. <https://doi.org/10.3390/colorants1020011>.
- [82] Garrudo-Guirado, M.L., Blanco-Flores, A., Toledo-Jaldin, H.P., Sánchez-Mendieta, V., Vilchis-Néstor, A.R., 2018. Reuse of sustainable materials for xylenol orange dye and copper (II) ion ammoniacal removal. *J Environ Manag* 206, 920–928. <https://doi.org/10.1016/J.JENVMAN.2017.11.074>.
- [83] Mani, S., Bharagava, R.N., 2016. Exposure to crystal violet, its toxic, genotoxic and carcinogenic effects on environment and its degradation and detoxification for environmental safety. in: *Rev. Environ. Contam. Toxicol*. Springer, Cham, pp. 71–104. https://doi.org/10.1007/978-3-319-23573-8_4.
- [84] Robens, J.F., Dill, G.S., Ward, J.M., Joiner, J.R., Griesemer, R.A., Douglas, J.F., 1980. Thirteen-week subchronic toxicity studies of Direct Blue 6, Direct Black 38, and Direct Brown 95 dyes. *Toxicol Appl Pharmacol* 54, 431–442. [https://doi.org/10.1016/0041-008X\(80\)90170-2](https://doi.org/10.1016/0041-008X(80)90170-2).
- [85] Pan, H., Feng, J., Cerniglia, C.E., Chen, H., 2011. Effects of Orange II and Sudan III azo dyes and their metabolites on *Staphylococcus aureus*. *J Ind Microbiol Biotechnol* 38, 1729–1738. <https://doi.org/10.1007/S10295-011-0962-3>.
- [86] Khayyat, L.L., Essawy, A.E., Sorour, J.M., Soffar, A., 2018. Sunset Yellow and Allura Red modulate Bcl2 and COX2 expression levels and confer oxidative stress-mediated renal and hepatic toxicity in male rats. *PeerJ* 6. <https://doi.org/10.7717/PEERJ.5689>.
- [87] Hashem, E.Y., Saleh, M.S., Al-Salahi, N.O.A., Youssef, A.K., 2017. Advanced spectrophotometric analysis of sunset yellow dye E110 in commercial food samples. *Food Anal Methods* 10, 865–875. <https://doi.org/10.1007/s12161-016-0630-3>.
- [88] John, E., Ashitha, V.C., 2010. Acute toxic effects of the textile dye, acid blue 113, on the biochemicals of teleost fish, *Tilapia mossambica* (Peters) (Pisces:Teleostei, Cichlidae). *Biosci. Biotechnol. Res. Asia* 7, 395–400.
- [89] Scientific Committee on Consumer Safety, Revision of the opinion on Acid Orange 7 - SCCS/1536/14, 2014. <https://doi.org/10.2772/48921>.
- [90] Joseph, J., Radhakrishnan, R.C., Johnson, J.K., Joy, S.P., Thomas, J., 2020. Ion-exchange mediated removal of cationic dye-stuffs from water using ammonium phosphomolybdate. *Mater Chem Phys* 242, 122488. <https://doi.org/10.1016/j.matchemphys.2019.122488>.
- [91] Sun, X., Chen, J.H., Su, Z., Huang, Y., Dong, X., 2016. Highly effective removal of Cu(II) by a novel 3-aminopropyltriethoxysilane functionalized polyethyleneimine/sodium alginate porous membrane adsorbent. *Chem Eng J* 290, 1–11. <https://doi.org/10.1016/J.CEJ.2015.12.106>.
- [92] Dávila-Guzmán, N.E., Cerino-Córdova, F.J., Díaz-Flores, P.E., Rangel-Mendez, J.R., Sánchez-González, M.N., Soto-Regalado, E., 2012. Equilibrium and kinetic studies of ferulic acid adsorption by Amberlite XAD-16. *Chem Eng J* 183, 112–116. <https://doi.org/10.1016/J.CEJ.2011.12.037>.
- [93] Illanes, C.O., Ochoa, N.A., Marchese, J., 2009. Kinetic sorption of Cr(VI) into solvent impregnated porous microspheres. *Chem Eng J* 136, 92–98. <https://doi.org/10.1016/J.CEJ.2007.03.008>.
- [94] Üzümlü, G., Özmen, B.A., Akgül, E.T., Yavuz, E., 2022. Emulsion-templated porous polymers for efficient dye removal. *ACS Omega* 7, 16127–16140. https://doi.org/10.1021/ACSOMEGA.2C01472/ASSET/IMAGES/LARGE/AO2C01472_0011.JPEG.
- [95] Vallejos, S., Reglero, J.A., García, F.C., García, J.M., 2017. Direct visual detection and quantification of mercury in fresh fish meat using facilely prepared polymeric sensory labels. *J Mater Chem A* 5, 13710–13716. <https://doi.org/10.1039/c7ta03902f>.
- [96] Deshannavar, U.B., Kumar Singa, P., Gaonkar, D., Gayathri, A., Patil, A., Malade, L.V., 2020. Removal of acid violet 49 and acid red 88 dyes from aqueous solutions using advanced oxidation process. *Mater Today Proc* 24, 1011–1019. <https://doi.org/10.1016/j.matpr.2020.04.414>.